8. Force and Moment Measurement

Measurement of steady and fluctuating forces acting on a body in a flow is one of the main tasks in windtunnel experiments. In aerodynamic testing, strain gauge balances will usually be applied for this task as, particularly in the past, the main focus was directed on the measurement of steady forces. In many applications, however, balances based on piezoelectric multicomponent force transducers are a recommended alternative solution. Contrary to conventional strain gauge balances, a piezo balance features high rigidity and low interferences between the individual force components. High rigidity leads to very high natural frequencies of the balance itself, which is a prerequisite for applications in unsteady aerodynamics, particularly in aeroelasticity. Moreover for measurement of extremely small fluctuations, the possibility exists to exploit the full resolution independently from the preload.

Concerning the measurement of small, steady forces, the application of piezo balances is restricted due to a drift of the signal at constant load. However, this problem is not as critical as generally believed since simple corrections are possible.

The aim of this chapter is to give an impression of the possibilities, advantages and limitations offered by the use of piezoelectric balances. Several types of external balances are discussed for wall mounted models, which can be suspended one-sided or twin-sided. Additionally an internal sting balance is described, which is usually applied inside the model. Reports are given on selected measurements performed in very different windtunnels, ranging from low-speed to transonic, from short- to continuous running time and encompassing cryogenic and high pressure principles. The latter indicates that special versions of our piezo balances were applied down to temperatures of –150 °C and at pressures of up to 100 bar.

The projects span from a wing/engine combination in a low-speed wind tunnel to flutter tests with a swept-wing performed in a Transonic Wind Tunnel, and include bluff bodies in a high pressure and cryogenic windtunnel, as well. These tests serve as examples for discussing the fundamental aspects that are essential in developing and applying piezo balances. The principle differences between strain gauge balances and piezo balances will also be discussed.

8.1 Steady and Quasi-Steady Measurement

The key measurement system in a wind tunnel is the multi-component force and moment measurement instrumentation. More than 70% of the tests in a wind tunnel require some kind of force measurements. Historically the instruments were purely mechanical and their mechanism resembled balances for weighing; hence the use of the term *balance* today. Today these balances are often based on transducers or are constructed out of a single piece of metal, on which strain gauges are applied. All balances must have a minimum of one sensing element for every component to be measured. The strain sensor usually is a resistance foil strain gauge, but also semiconductor gauges are used. Illustrated in Fig. 8.1 is one of the first wind tunnel balances built by Gustav Eiffel in 1907. The man on the upper gallery was responsible for balancing the lift generated by the airfoil in the tunnel below and simultaneously recording its associated lift.

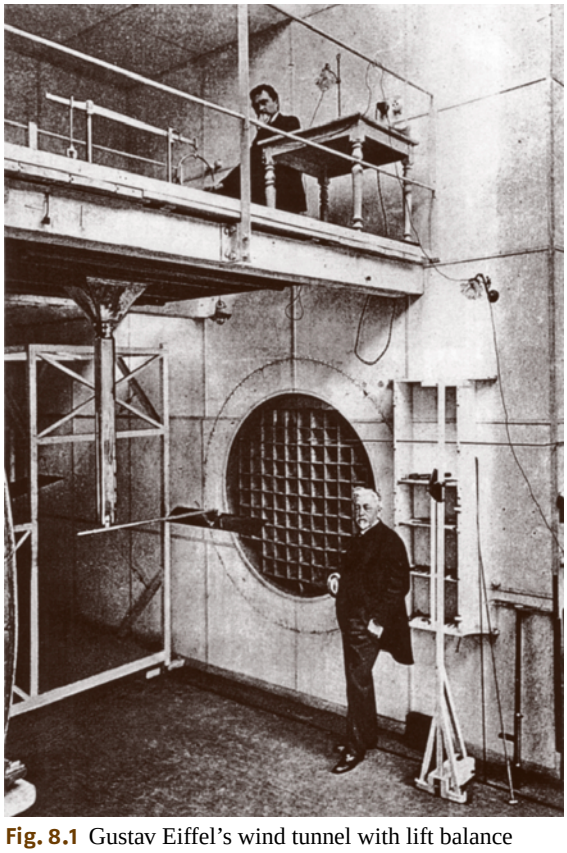

Fig. 8.1 Gustav Eiffel's wind tunnel with lift balance

8.1.1 Basics

Balance Types

Balance types are distinguished by the number of force/moment components which are measured simultaneously – one to six are possible – and the location at which they are placed. If they are placed inside the model they are referred to as *internal balances* and if they are located outside of the model or the wind tunnel, they are referred to as *external balances*.

External Balances

Two types of external balances exist. The first is the one-piece external balance, which is constructed from one single piece of material and which is equipped with strain gauges. Such balances are also referred to as *sidewall balances* as used in half-model tests.

The second type of external balance comprises single force transducers which are connected by a framework. Such a design can be built very stiff but needs more space compared to the one-piece design. However, there is usually plenty of space available around the wind tunnel for such a balance, and so the construction can be optimized with respect to measurement requirements, such as optimized sensitivity, stiffness and decoupling of load interactions.

Internal Balances

There is limited space inside the model itself, so internal balances have to be relatively small in comparison to external balances. There are two main types of internal balances. The monolithic type, in which the balance body consists of a single piece of material, is designed in a way such that certain areas are primarily stressed by the applied loads. The other internal balance type uses small transducers which are orientated with their sensing axes in the direction of the applied loads. Such a balance is combined into a solid structure. A balance measures the total model loads and therefore is placed at the center of gravity of the model and is generally constructed from one solid piece of material.

Loads

In this chapter the word *load* will be used to describe both the applied forces and moments. The task of a balance is to measure the aerodynamic loads, which act on the model or on components of the model itself. In total there are six different components of aerodynamic loads, three forces in the direction of the coordinate axes

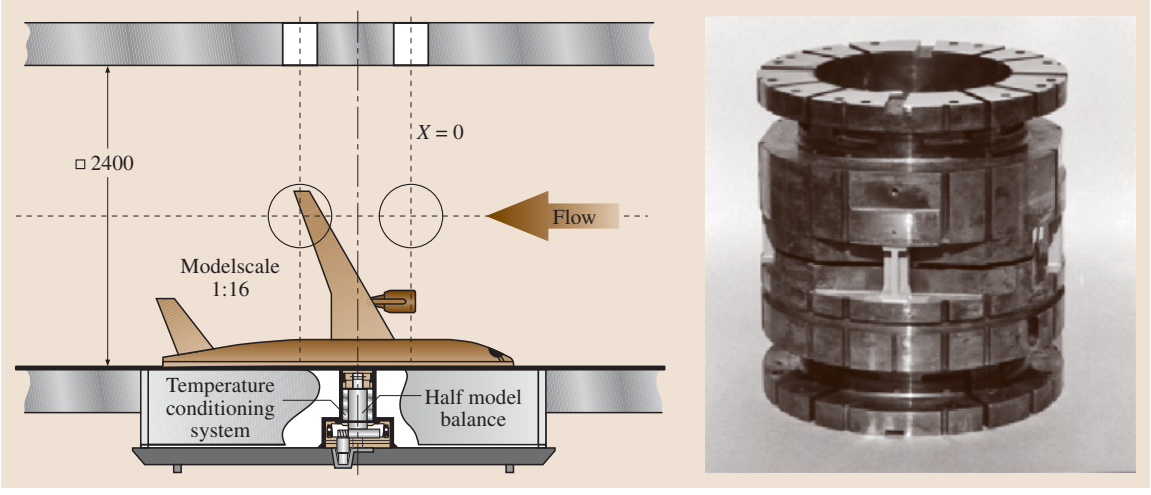

Fig. 8.2 Side-wall balance test configuration (*left*), and typical side-wall balance (*right*)

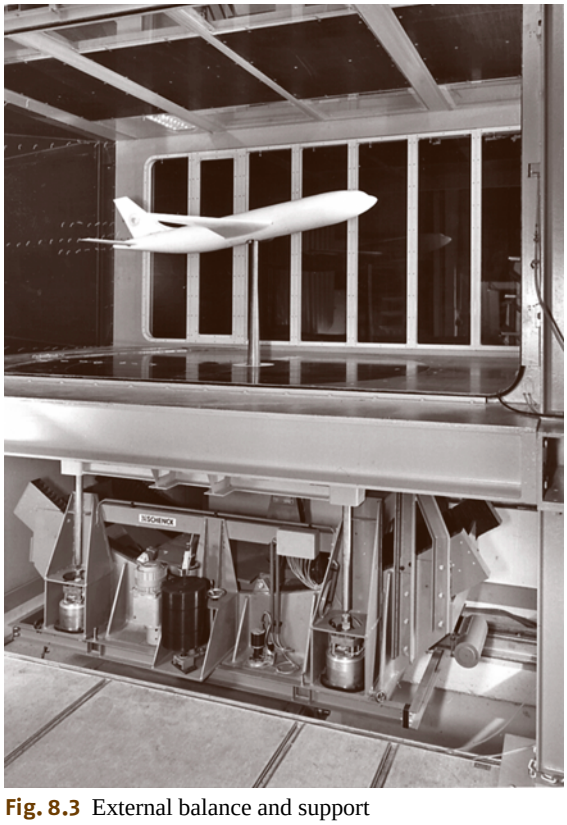

Fig. 8.3 External balance and support

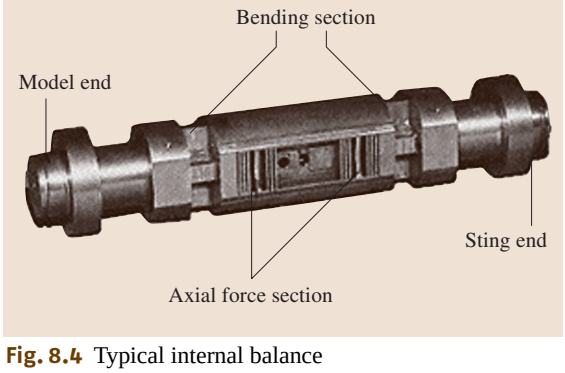

Fig. 8.4 Typical internal balance

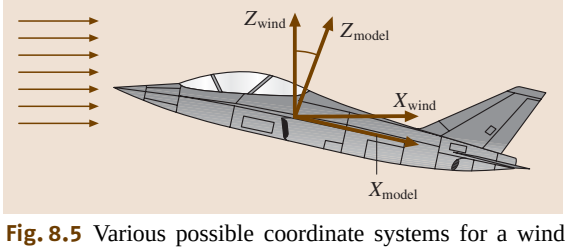

Fig. 8.5 Various possible coordinate systems for a wind tunnel and model

and the moments around these axes themselves. These components are measured in a certain coordinate system which can be either fixed to the model or to the wind tunnel. For the measurement of loads on model parts such as rudders, flaps and missiles, normally less than six components are required.

Definition of Coordinate Systems

One possible coordinate system is fixed to the wind tunnel – the wind axis system – and is aligned to the main

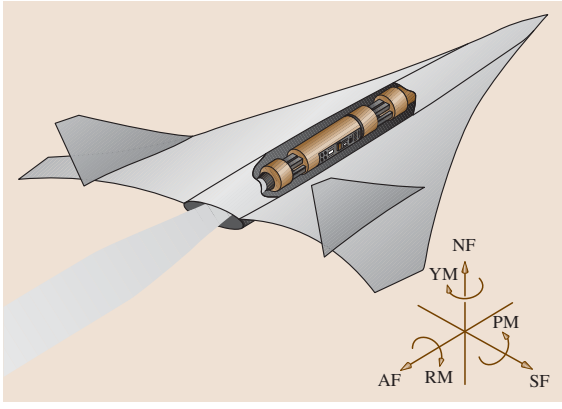

Fig. 8.6 Definition of wind axis system in the USA

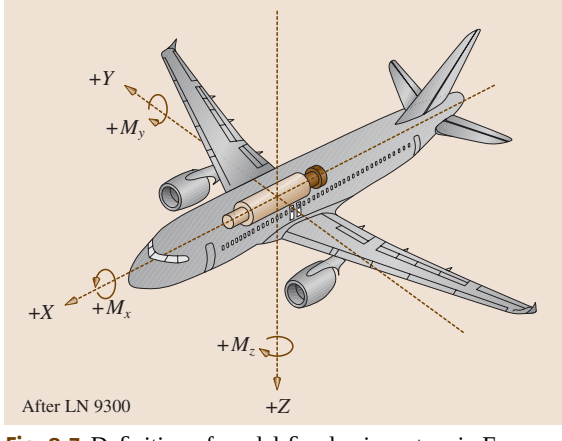

Fig. 8.7 Definition of model-fixed axis system in Europe

flow direction. The lift force is generally defined as the force on the model acting vertical to the main flow direction whereas the drag is defined as the force acting in the main flow direction. This definition is common all over the world. However, the definition of the positive direction of the forces is not universal. Whereas lift (normal force) and drag (axial force) are defined positive in the USA (Fig. 8.6), in Europe (Fig. 8.7) weight and thrust are defined as positive in the wind axis system.

To form a right-hand axis system, the side force in the USA has to be positive in the starboard direction. The definitions of the positive moments do not follow the sign rules of the right-hand system. The pitching moment is defined as positive turning right around the y-axis, but yawing and rolling moments are defined positive turning left around their corresponding axes. This makes this system inconsistent in a mathematical sense.

Table 8.1 Definition of positive axis direction

Balance Axis System	Name of Component	European	USA
		Positive direction	Positive direction
X	Axial force	In flight	In wind
Y	Side force	To starboard	To starboard
Z	Normal force	Down	Up
M_x	Rolling moment	Roll to starboard	Roll to starboard
M_y	Pitching moment	Turn up	Turn up
M_z	Yawing moment	Turn to starboard	Turn to starboard

The European axis system is a consistent with the right-hand system and the definition is based on a standard given by DIN-EN 9300 or ISO 1151. A balance which always stays fixed in the tunnel, and relative to the wind axis system, always gives the pure aerodynamic loads on the model.

In the case of the model-fixed axis system, the balance does not measure the aerodynamic loads directly. The loads acting on the model are given by the balance and the pure aerodynamic loads must then be calculated from these components by using the correct yaw and pitch angles. The difference between American and European definitions of the positive direction remains the same in this case.

Specification of Balance Load Ranges

Before a balance can be designed, the specifications of the load ranges and the available space for the balance are required. This is a challenging step prior to the design of a balance since cost and accuracy considerations must be made long before the first tests are performed.

The maximum combined loads specify the load ranges for the balance design. The maximum design loads of a balance are defined in various manners. For example, if several loads act simultaneously, then the load range must be specified as the *maximum combined load*. If the maximum load acts alone, the load range is defined then as the *maximum single load*. Usually such single loads do not exist in wind tunnel tests and combined loads must be expected. Such combined loads stress the balance in a much more complicated manner and therefore deserve very careful attention. The stress analysis of the balance has to take into account this situation. Furthermore, the combination of two loads

Table 8.2 Determination of maximum combined loads for an external balance

			Wind axis system							Model axis system					
Test type	q	A	C_x	C_y	$C\ldots$	Drag	Side Force	$F\ldots$, $M\ldots$	max α, β, γ	F_x	F_y	F_z	M_x	M_y	M_z
	(Pa)	(m^2)				(N)	(N)	(N), (N m)	(deg)	(N)	(N)	(N)	(N m)	(N m)	(N m)
Full model															
Half model															
etc.															

usually requires that the balance carries higher loads. To determine which balance can be used for a given setup, the balance manufacturer provides the test engineer with loading diagrams which define the maximum load combinations for various available models.

In the case of external balances the available space is usually not a limiting factor. External balances are often used over several decades in a wind tunnel and therefore specifications of the design load ranges are orientated more to the capabilities of the wind tunnel itself and the associated model setups such as half-model and full-model tests, or the possibility of aircraft, car and building testing. For the design of an external balance, first load ranges of the principle balance configuration must be defined. Two different options are possible:

The first option is to mount the turntable inside the weigh bridge. In this case the balance stays in the wind axis system and therefore the balance always measures the wind loads. The disadvantage of this option is that the whole turntable mechanism has to be mounted on the metric side of the balance such that the balance is preloaded by the weight of this mechanism.

The second option is to mount the whole balance on a turntable. In this case some components stay in the wind axis system and some stay in the model axis system, so a calculation of the aerodynamic loads from the balance loads is necessary. For example, in the case of a full model setup, as shown in Fig. 8.9, the balance will always measure the aerodynamic loads when the angle of attack changes. In a half-model setup, as shown in Fig. 8.11, the balance will move with the model when the angle of attack changes and will measure the loads in the model axis system.

This makes the determination of the balance load ranges rather difficult. Therefore it is useful to fill out a table where first the maximum loads for the different test setups are calculated in the wind axis system. In order to do this some assumptions of the aerodynamic coefficients and the model size must be made. By assuming values for the maximum angle of attack or yaw angle, the maximum loads in the model axis system can be calculated.

From such a table the maximum of each component can be taken as the maximum load for the balance. Naturally this leads to a balance with a rather high load ranges and for some cases the load range could be too high to measure with high resolution. However, if a certain test requires a high resolution and this test is mostly performed in the tunnel, it is generally better to accept the lower load range to obtain higher resolution and higher accuracy. These considerations must be made for all components to ensure a balance with the best

Table 8.3 Determination of maximum combined load for an internal balance

			Wind axis system							Model axis system					
Test type	q	A	C_x	C_y	$C\ldots$	Drag	Side Force	$F\ldots$, $M\ldots$	max α, β, γ	F_x	F_y	F_z	M_x	M_y	M_z
	(Pa)	(m^2)				(N)	(N)	(N), (N m)	(deg)	(N)	(N)	(N)	(N m)	(N m)	(N m)
Transporter															
Landing															
Cruise															
Combat															
Other															

fit of the load range for the normal operation of the tunnel.

For an internal balance the available space is a major concern. The available space for balances is restricted by the diameter of the fuselage. As transport aircraft become larger, the scale for models also become larger, complicating matters since the cross sections of wind tunnels have not grown at the same rate as the aircraft. As a result the available diameter for internal balances has become smaller.

For combat aircraft the loads in relation to the available space inside the model are very high. This is the case since the wind tunnel tests for this type of aircraft are mostly performed in pressurized wind tunnels to obtain the correct Mach number. The high static pressure leads to relatively high loads on the model in comparison to tests at atmospheric pressure.

These two effects lead to higher specific loads on the balance, making it much more complicated to develop a balance with high accuracy. Therefore the definition of the load ranges and the definition of the available space must be performed very carefully to ensure a high quality balance design.

The specification for an internal balance should therefore be made related to the model and the loads on this model during the tests, and not on the tunnel capabilities themselves. If these specifications are not carefully performed, the internal balances will provide insufficient sensitivity and accuracy for the tests.

Unlike an external balance, where some of the components are always fixed to the wind axis system, the internal balance always measures the loads in the model axis system and therefore the lift and drag are always a combination of the axial and normal forces. Because of this, the angle of attack at which maximum loading occurs must be taken into account. For combat aircraft maximum loads can act at an angle of attack as high as 40°, whereas the maximum forces for a clean transport aircraft occur in and around an angle of attack of 15°.

Because an internal balance is mounted inside the model and does not change in orientation relative to the model itself, no maximum single load occurs. For different test setups (transporter, combat, high-lift, cruise-condition, etc.) different maximum combined loads occur, so it is also useful to prepare a table to determine the maximum combined loads on the balance.

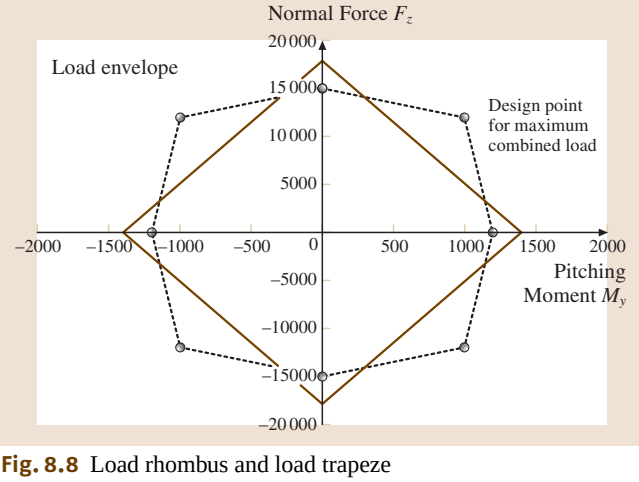

Fig. 8.8 Load rhombus and load trapeze

Maximum Combined Load: Maximum Single Load

The definition of the maximum load can differ between a combined load acting simultaneously, termed maximum combined load, and a maximum load acting alone, defined as the maximum single load. The maximum single load forms a load trapeze, which does not automatically cover the test requirements (Fig. 8.8). The maximum combined load specifies the load range for the balance design. Usually single loads do not occur in wind tunnel testing. Combined loads stress the balance in a much more complicated way, so the stress analysis of the balance has to take this situation into account. With the combination of only two loads the balance usually can carry higher loads than defined by the maximum combined loading. To estimate which load can be carried for a given situation the balance manufacturer provides a loading diagram (load rhombus) which allows the test engineer to judge whether the load combination of the planned test is within the limits of the balance.

Which one of the above mentioned loads is used as the "full-scale load" depends on the balance manufacturer's philosophy. The user should specify the definition of the full scale load, because by definition the relative uncertainty of the balance can vary by a factor of two without any difference in the absolute uncertainty. This is discussed in detail in the following section.

8.1.2 Basic Terms of Balance Metrology

In this chapter brief definitions are given of the terms used. Most of these terms are defined in some international standard such as the "*Guide of uncertainties in measurement (GUM)*" [8.1] or in the case of the United States, the AIAA Standards documented in *Assessment of Experimental Uncertainty with Application to Wind Tunnel Testing* [8.2] and the *Calibration and Use of In-*

ternal Strain Gauge Balances with Application to Wind Tunnel Testing [8.3].

Full Scale Load or Output. Full scale load or output can be interpreted in several ways. The most obvious definition is the maximum combined load or the signal corresponding to this load. It is also possible to define the full scale load or output as the maximum of the single loads. The maximum single loads are usually much higher than the maximum combined loads, so uncertainties related to these values are much smaller than those related to the maximum combined loads. This has to be taken into account if balances from different manufactures are compared. However, for a particular wind tunnel test the maximum of the single loads seldom occur and the use of maximum combined loads or signals as the full scale reference yields much more realistic information about the accuracy of the balance.

Systematic Errors or Bias of an Instrument. Systematic errors are repeatable errors which occur at every measurement. If the cause of a systematic error can be detected, it can be eliminated by calibration or compensation. If the source of a systematic error can not be detected under repeatable conditions it is then simply accepted as the difference between the measured value and the true value.

Random Errors. Random errors are defined as the difference between the mean value of an infinite number of measurements under repeatable conditions and a single measurement. The value of the random error is equal to the difference between the total error minus the systematic error.

Resolution. Resolution is the smallest value which can be detected by a balance. Similarly it can be defined as the smallest detectable difference between two loads. The maximum resolution should be in the range of 0.005% of the full scale load. For a normal wire strain gauge, resolution in this range is not a problem and the limits of the resolution are given by the measuring equipment. Good equipment today offers a resolution of less than 0.0003% of the full scale load. Effectively the more money one spends on the equipment, the better the obtainable resolution.

Repeatability. If a certain balance loading is repeated after a certain amount of time, the repeatability is measured as the difference in the two signals. This is a very important characteristic for a balance, since many tests in a wind tunnel compare different model configurations. Most often wind tunnel tests can not exactly reproduce conditions found in reality. This means that if the test itself does not represent reality yet the engineers attempt to compare the difference between two designs under wind-tunnel test conditions, the extrapolation of results to reality can be very challenging. Repeatability can be as good as the resolution but is usually worse. The repeatability of a good balance is in the range of 0.005% of the full scale load. Repeatability depends also on time, so it is distinguished between short-term repeatability, for example between two wind tunnel runs, and long-term repeatability, which is for example the difference between two complete wind tunnel installations. Both short- and long-term repeatability are of equal importance since the loads on a new aircraft as well as the loads on an older aircraft design must be measured with the same accuracy as the differences between the new model configurations. The main challenge often is the discrepancy in the flow parameters between model and reality, especially Reynolds number. Most of the uncertainty in the force prediction on the real aircraft is then caused by this Reynolds number gap, therefore relative measurements to the model of an older aircraft design are used to reduce this level of uncertainty.

Interactions and Interference. One of the major systematic errors of a wind tunnel balance is caused by the interactions or interference of the model with surrounding components. For example, the sensor measuring the axial force might also pick-up the loads from other components. This additional signal can be several percent of the measured axial force signal. As mentioned above, such a systematic error can be corrected through proper calibration.

Accuracy. The term accuracy is very broad and generally describes the agreement between the measured data, in this case the wind tunnel test data, and the true value which will be measured in the flight test after wind tunnel testing is complete. There are many influencing factors, such as the measurement of static and dynamic pressure, wall and sting interactions, precision of model geometry, flow quality, angle of attack and balance uncertainty. Since there are so many potential errors, it becomes difficult to specify the accuracy for a wind tunnel test. Balance uncertainty alone must be taken into account through balance calibration.

Absolute Error and Uncertainty. The absolute error is defined as the difference between the real load acting on

the model (true value) and the load detected by the balance. Normally the true value is unknown; therefore in practice a "conventional true value" is used. Besides all the error sources in the instrumentation and the balance, the error of the load measurement is strongly influenced by the balance calibration, since in this process the relation between the signals of the balance and the true loads are determined. According to the *"Guide to the Expression of Uncertainties in Measurement"* [8.1], often abbreviated as *GUM*, the absolute error is defined as the uncertainty of the measurement and can be given as the experimental standard deviation of the whole process. For a given wind tunnel test the uncertainty of the measured data is not only dependent on the measurement of the loads, but also influenced by the measurement of the angle of attack, the dynamic pressure, the model geometry, the flow quality and all the instrumentation which are used to determine the aerodynamic performance and associated derivatives. Regarding the desired precision of the test result, minimum requirements for the load measurement can be estimated from flight test data of an existing aircraft.

Accuracy Requirements. The requirement placed on accuracy is a function of the price of the balance. If a balance is specifically designed and built for one particular set of wind-tunnel tests, it should be only as accurate as those tests require. This is however not usually the case. The high cost of balance construction usually restricts a given tunnel to a small number of balances, which should ideally cover the range of test capabilities for that particular tunnel. An estimate of the maximum required accuracy for the development of transport aircraft [8.4, 5] can be made by defining which differences between a developed aircraft and the new aircraft are to be investigated. The usual outcome of such an accuracy requirement study is that the balance must be able to measure a difference of 1 to 2 drag counts, which is equal to an accuracy requirement of the balance of better than 0.07% to 0.1% of the full scale load. This value is a global one yet should be specified for every new test setup.

8.1.3 Mounting Variations

When using external balances, there are many different possibilities for mounting the models. For example, a full model aircraft can be supported by a three-sting arrangement (Fig. 8.9) or a central sting (Fig. 8.10). For cars and buildings more than three supports are sometimes necessary. The external balance support system should provide for as many arrangements as possible.

The struts on the wing support the model at the quarter-chord positions and carry most of the load, except for the pitching moment which is balanced by the strut at the tail of the model. All links to the model are jointed around the *y*-axis, so that a vertical movement of the tail strut allows for easy variation of the angle of attack. Yaw angles are set by moving the whole setup on the turntable.

Using the central-sting mounting the model is fixed inside the fuselage in all directions. The adjustment of the angle of attack is done through *y*-axis mechanism inside the fuselage. All loads must be carried by this support and therefore must be very rigid to minimize dynamic movements of the model during testing.

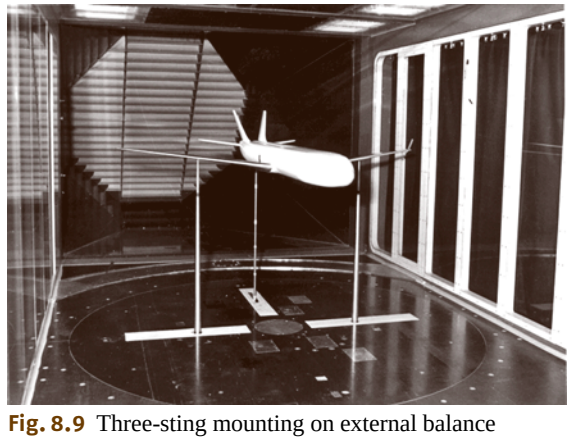

Fig. 8.9 Three-sting mounting on external balance

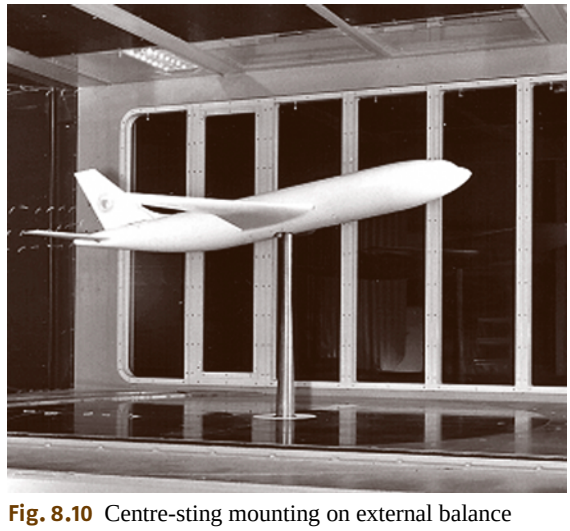

Fig. 8.10 Centre-sting mounting on external balance

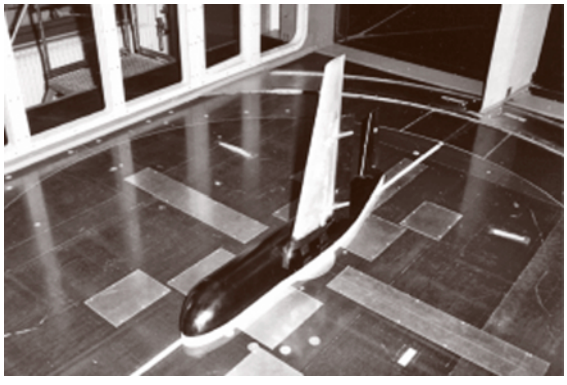

Fig. 8.11 Semi-span models on external balance

Fig. 8.14 Twin-sting rig with dummy tail sting

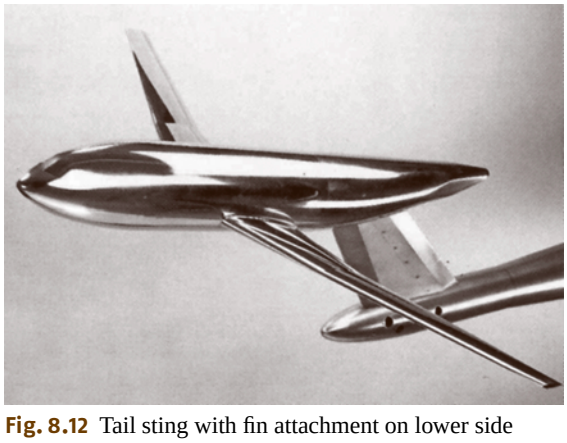

Fig. 8.12 Tail sting with fin attachment on lower side

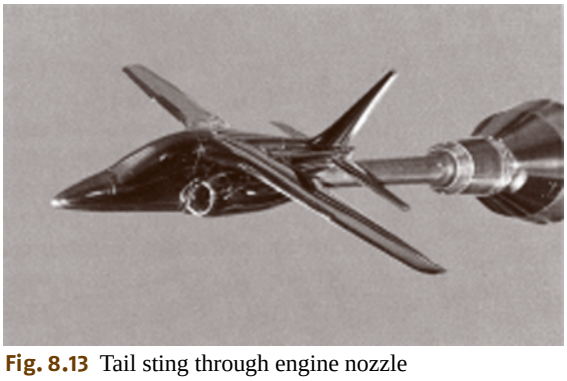

Fig. 8.13 Tail sting through engine nozzle

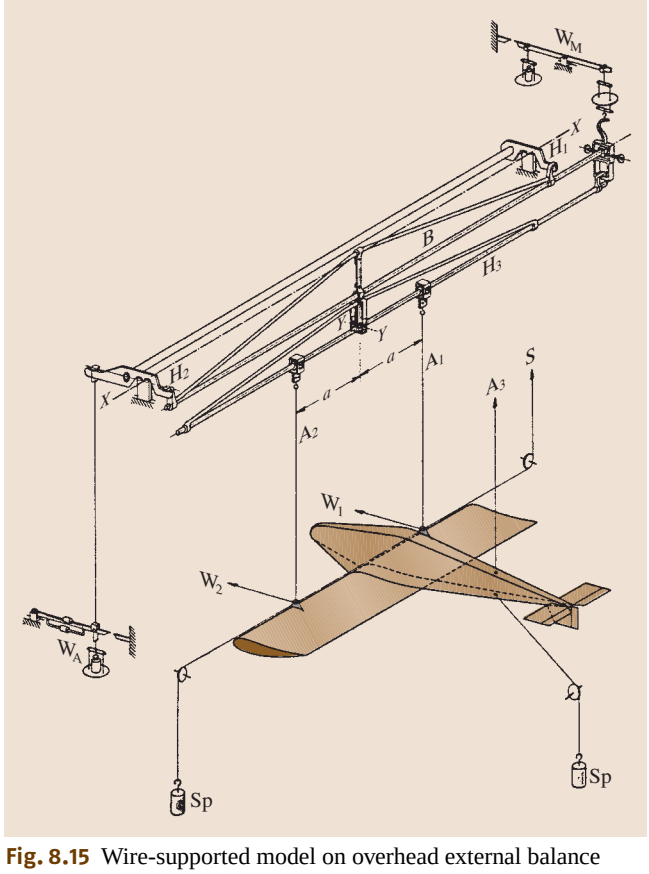

Fig. 8.15 Wire-supported model on overhead external balance

Semi-span models (Fig. 8.11) are used to increase the effective Reynolds number of the tests by increasing the geometry of the model. Besides the higher Reynolds number, the lager model size makes the models with variable flaps and slats much easier to construct, thus semi-span models are often used for the testing of take-off and landing configurations.

The most common setup using an internal balance is the back-sting arrangement (Fig. 8.13), in which the

and the attachment point of the beam. If a force is not applied at the point where the calibration load is applied one will produce errors proportional to this misalignment. This problem can be overcome by using a different transducer design. Some possible designs are shown in Fig. 8.27. Their common design principle is that two bending beams should be coupled forming a parallelogram. If the coupling element is stiff enough the load attachment point remains vertical, such that the transducer signal does not depend on the distance between this point and the gauge area.

Load cells which use the shear stress to determine either an applied force or a torque moment do have the same principle advantage that within the gauge area a positive and a negative shear stress is generated with the same magnitude. Therefore this type also has a linear output proportional to the applied load.

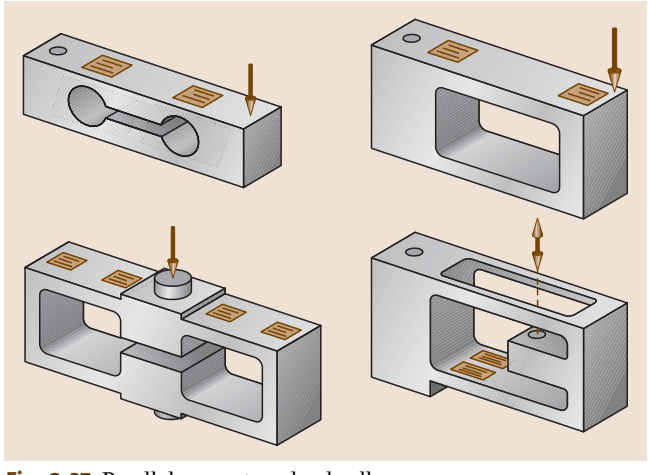

Fig. 8.27 Parallelogram-type load cells

Shear-type load cells

The maximum shear stress on a cantilever beam (Fig. 8.28), produced by force (F), appears at the center line of the beam at $(45\pm w)°$here the tension of compression stresses are nearly zero. In such a case the maximum strain also appears at $(45\pm,)°$ therefore to get the maximum output the gauges must be bonded as is shown in Fig. 8.28. The dimensions of the beam can be calculated by determining the stresses in $\tau_{max} = Fc/A$ [N/mm^2], where F is the applied force, $A = bh$ [mm^2] the beam cross section and c is a form factor which depends on the shape of the beam cross section. For a rectangular cross section $b \leq h/2$ and $c = 3/2$, whereas for a circular cross section $c = 4/3$. These formulas are approximations for the centerline. The strain gauge covers a certain area around the centerline such that the integrated value measured by the strain gauge will be smaller. The signal of the transducer can be determined using the equation $\Delta U/U = k\varepsilon_{45°}$ for the full bridge output as well as the equation $\varepsilon_{45°} = \tau_{max}/2G$ for the strain under the gauge.

For a torque transducer the shear stress must be calculated using $\tau_{max} = M_t/W_p$ [N/mm^2], where M_t [Nm] is the torque moment and W_p [mm^3] is the polar section modulus.

Tension and Compression Load Cells

The main difference between shear- and bending-stress transducers and load cells using tension and compression stress measurements is that in the case of the latter there is no positive and negative stress of equal value. If the tension stress $\sigma_{tension} = F/A$ is defined as positive, the negative compression stress becomes $\sigma_{comp} = \nu F/A$, termed the Poisson stress. For metals $\nu = 0.3$ while the compression stress is only about 1/3 of the tension stress. Using a Wheatstone bridge with four gauges applied, as shown in Fig. 8.30, the output of such a transducer related to the force (F) will be nonlinear. This is not a big disadvantage as long as these nonlinearities are taken into account through calibration.

For standard load cells a nonlinear characteristic is not very common, however for applications in wind-tunnel testing they are some times advantageous since they do not require much space. Another advantage of

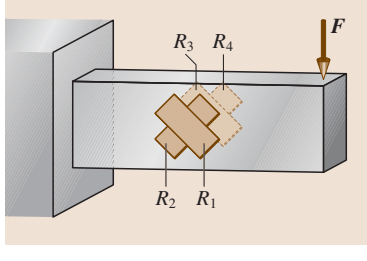

Fig. 8.28 Shear-type load cells

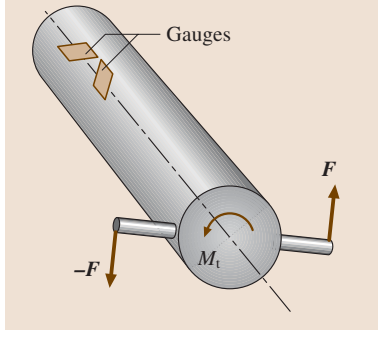

Fig. 8.29 Torque transducer

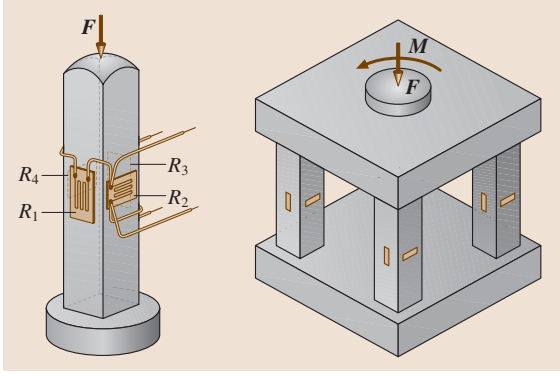

Fig. 8.30 Tension-type load cell (*left*) and cage of tension and compression columns (*right*)

such a transducer is that the strain gauges are placed very close to each other, thus remaining at the same temperature level. This minimizes the zero-drift and temperature-gradient sensitivity of the transducer. In some wind-tunnel balances such tension and compression columns can be arranged in a cage. In such a way it is possible to measure tension and compression as well as the moments acting on the metric side of the transducer.

8.1.12 Multi-Component Load Measurement

The fundamental criterion of all multi-component load measurements is that all the loads acting on a model must be separated into single components as best as possible. In order to measure each single component at least one associated transducer per component must exist. This criterion can be best fulfilled in external wind-tunnel balances, where plenty of space is available to separate the load by decoupling rods with flexures. Sting balances are much smaller and so this criterion can be only partially fulfilled. Consequently, interactions or interferences in the measurement of the different components must exist.

The interactions inside a balance are systematic errors which can be determined through calibration. Therefore it is often necessary to measure more components in order to separate the errors during calibration. Another reason for having more measurement sections than components is to measure the errors caused by temperature gradients inside the balance. Temperature gradients cause deflections of the metric part against the non-metric part which in turn are measured by the strain gauges. This is also a systematic error which can be separated through calibration. In order to extract the loads from the balance signals, the following equation must be resolved:

$$\boldsymbol{F} = \overline{E}\boldsymbol{S}\,, \tag{8.25}$$

where $\boldsymbol{F}$ is the force vector, $\overline{E}$ is the evaluation matrix and $\boldsymbol{S}$ the signal vector.

Through calibration one obtains an evaluation matrix whose elements take all the interactions and systematic errors into consideration. For a balance with no interactions, the six sensitivities for each component are the diagonal of the evaluation matrix while all other elements become zero. For a balance where nonlinearities up to the third order are considered, the evaluation matrix consists of $6 \times 33 = 198$ elements.

8.1.13 Internal Balances

Two general groups of internal balances exist. The first group consists of the so-called box balance. These can be constructed from one solid piece of metal or can be assembled out from several parts. Their main characteristic is that their outer shape most often appears cubic, such that the loads are transferred from the top to the bottom of the balance. The second type of internal balance is termed sting balance. These balances have a cylindrical shape such that the loads are transferred from one end of the cylinder to the other in the longitudinal direction. Both one-piece and multi-piece sting balances exist.

Sting Balances

Internal sting balances are divided into two different groups. One group is the force-balance type and the other group is the moment-balance type. If the bridge output is directly proportional to one load component then these balances are termed *direct read balances*. Typically for all groups, the axial force and rolling moment are directly measured with one bridge. The measurements of lift force and pitching moment or for side force and yawing moment are done in different ways characterizing each group.

Moment-type balances and force-type balances have one main feature in common, being the lack of a direct

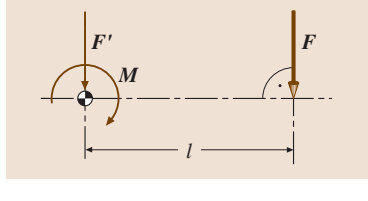

Fig. 8.31 Separation of force and moment

output proportional to lift/pitch and side force/yaw. The signals which are proportional to each of these loads must be then calculated by summing or subtracting the signal from one another, before being fed into the data reduction process. The advantage is that the associated concentrated wiring on each section is much less sensitive to temperature effects.

Force Balances. This type of balance uses two measurement sections placed in both the forward and the aft section of the balance. In these measurement sections a forward and aft force is measured most often through tension and compression transducers. These forward and aft force components are used to calculate the resulting force in the plane as well as a moment around the axis (perpendicular to the measurement plane). An example of a typical force balance is shown in Fig. 8.32.

Moment-Type Balances. Moment-type balances have a bending moment measuring section in the front as well as in the aft regions of the balance (S_1 and S_2 in Fig. 8.33).

The measurement of the two bending moments (S_1 and S_2) is used to obtain a signal which is proportional to the force in the measurement plane and a second one which is proportional to the moment around the axis (perpendicular to the measurement plane). The stress distribution shows that the moment M_y (M_z) is proportional to the sum of S_1 and S_2. However, the force F_y (F_z) is proportional to the difference in the signals S_1 and S_2.

To measure the rolling moment (M_x) one bending section must be applied with shear stress gauges to detect the shear stress τ. The most complicated part of the balance is the axial force section which consists of flexures and a bending beam to detect axial force. These flexures enable axial movement whilst carrying the other loads.

Direct-Read Balances. A direct-read balance can be categorized as either a force-balance type or as a moment-balance type. Instead of measuring a force or a bending moment at each section separately, half bridges on every section are directly wired to a moment bridge while the other set of half bridges are directly wired to a force bridge. Thus the difference between direct-read balances and the other types is only in the wiring of the bridges. The disadvantage of such a wiring is the length of the wires from the front to the aft ends. Temperature changes inside these wires cause errors in the output signals.

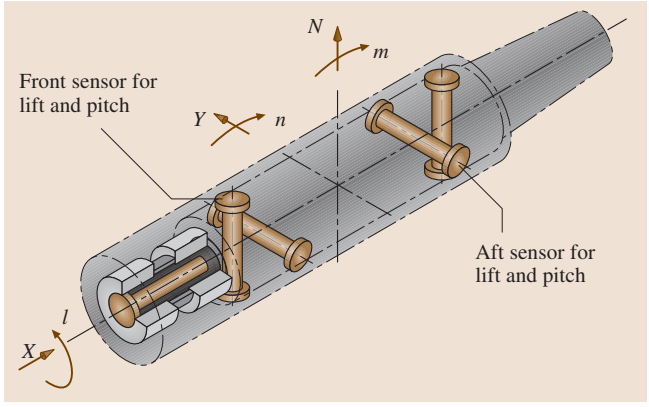

Fig. 8.32 Force balance with tension transducers in forward- and aft-sections (courtesy of Able Corp.)

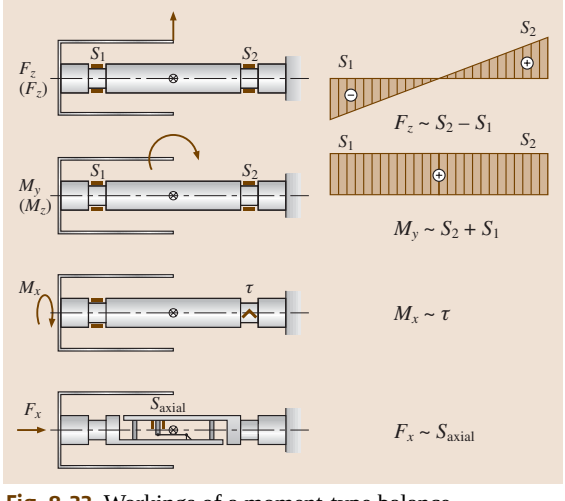

Fig. 8.33 Workings of a moment-type balance

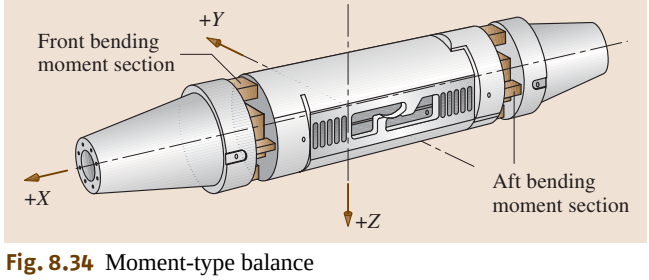

Fig. 8.34 Moment-type balance

Box Balances

The main difference between box balances and sting balances are the model and sting attachment area (Fig. 8.35). The load transfer in such balances is from

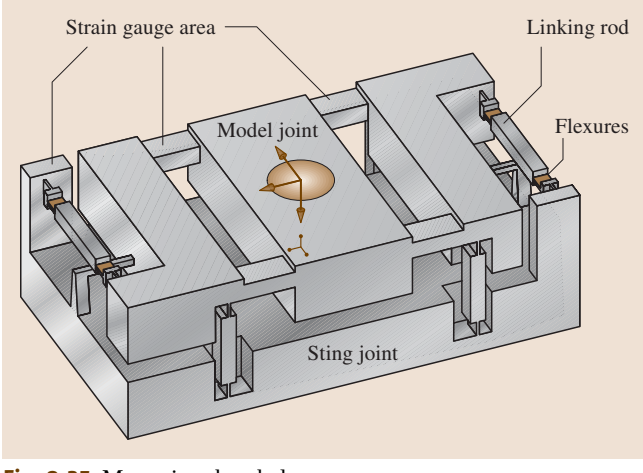

Fig. 8.35 Monopiece box balance

top to bottom along the vertical z-axis. Therefore these balances use a central sting arrangement, as shown in Fig. 0.30 for the case of an airplane configuration. The mono-piece balance is constructed from one single piece of material. The advantage of this relatively expensive manufacturing process is the low hysteresis and good creep behavior, which are basic requirements for good balance repeatability. Multi-piece box balances are built from several parts which can in turn be manufactured separately. The load transducers can either be integrated in the structure or separate load cells can be used instead. This enables a parallel manufacturing process with a final assembly at the end, in turn making the whole process quicker than that for a mono-piece balance. Box-type balances are considered internal balances, but have actually more in common with semi-span balances. In particular their temperature-sensitivity behavior is similar to that of semi-span balances.

Principle Design Equations

All internal balances measure the moment and the force in two different sections along the x-axis. The distance between the two sections defines the separation of the signal between force and moment. In the ideal case, half of the signal should be proportional to the force and the other half should be proportional to the moment.

To obtain the same output for the force and the moment, the distance $l = l_1 + l_2$ between the two sections has to be calculated. For a moment-type balance these relations can be described by the following equations

$$\sigma_1 = \frac{M_{B_1}}{W_1} = \frac{M + Nl_1}{W_1} ,$$

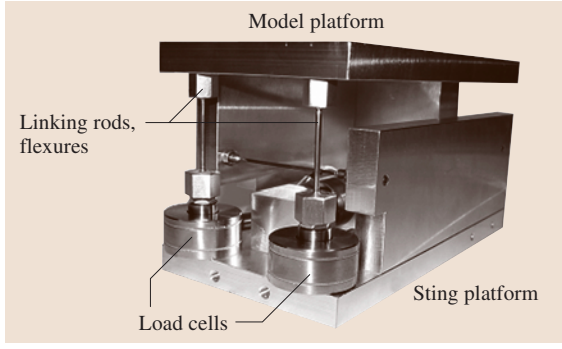

Fig. 8.36 Small-box balance with load cells

$$\sigma_2 = \frac{M_{B_2}}{W_2} = \frac{M - Nl_2}{W_2} , \quad W_1 = W_2 , \quad l_1 = l_2 , \tag{8.26}$$

where σ_1 and σ_2 are the stresses in sections one and two, respectively. These stresses are caused by the moment (M) and the force (N). W_1 and W_2 are the section moduli. The sum as well as the difference of these two stresses are

$$\sigma_1 + \sigma_2 = M\left(\frac{1}{W_1} + \frac{1}{W_2}\right) + N\left(\frac{l_1}{W_1} - \frac{l_2}{W_2}\right) = \frac{2M}{W} , \tag{8.27}$$

$$\sigma_1 - \sigma_2 = M\left(\frac{1}{W_1} - \frac{1}{W_2}\right) + N\left(\frac{l_1}{W_1} + \frac{l_2}{W_2}\right) = \frac{Nl}{W} . \tag{8.28}$$

In (8.27) it can be seen that the sum of the stresses is only proportional to the moment (M) and in (8.28) it can be seen that the difference of the stresses is only proportional to the force (N). Consequently the sum of the bridge signals S_1 and S_2 is proportional to the moment (M) while the difference of the bridge signal S_1

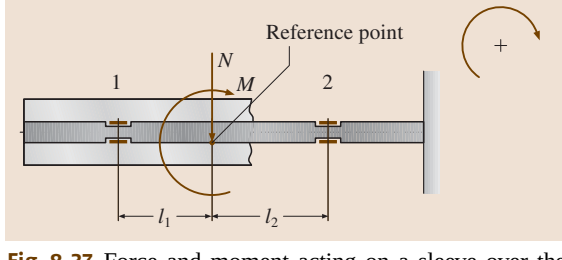

Fig. 8.37 Force and moment acting on a sleeve over the reference point

and S_2 is proportional to the force (N)

$$\sigma_1 + \sigma_2 \approx \Delta U_\mathrm{M}$$
$$\sigma_1 - \sigma_2 \approx \Delta U_\mathrm{N} \qquad (8.29)$$

At this point the ratio of the sum and the difference of the signals can be calculated

$$\frac{\Delta U_\mathrm{M}}{\Delta U_\mathrm{N}} = \frac{2M}{Nl} \,. \qquad (8.30)$$

For a given moment (M) and a given force (N), the aim is to have the ratio of the signal equal to one. The distance (l) between the measuring sections can be calculated in the following manner:

$$l = \frac{2M}{N} \,. \qquad (8.31)$$

This equation is also valid for force-type balances. Therefore for the same force and moment output, there exists an optimum distance between the measuring sections; thus the length of the balance can be in this way determined. If the required load combination results in a length that does not fit into the model, then the distance between the measuring sections must be compromised in such a way that the signals for the force or the moment are smaller than the other.

Another problem appears when the distance between lift and pitch in the $x-z$ plane is different than the distance between side force and yaw in the $y-x$ plane. One solution is to use different measuring sections, but this will enlarge the total length of the balance and is usually avoided.

For a single-test setup normally the balance length can be easily optimized for the model. However, the balance load range definition is more often a compromise between requirements for different test setups, where the maximum loads for all tests form the envelope of the combined-load range specification. In such cases very seldom can a good compromise for the balance dimensions be found.

Specific-Load Parameter. Before designing the bending section it is good to first determine whether the balance will have high loading or not. Loading in this case refers to the ratio between the loads and the available volume for the balance. This ratio expresses the magnitude of the stress level inside the balance before starting with the calculation. This ratio is also referred to as the *specific-load parameter*

$$S_\mathrm{round} = \frac{N + L/2 + M}{D^3} \,,$$

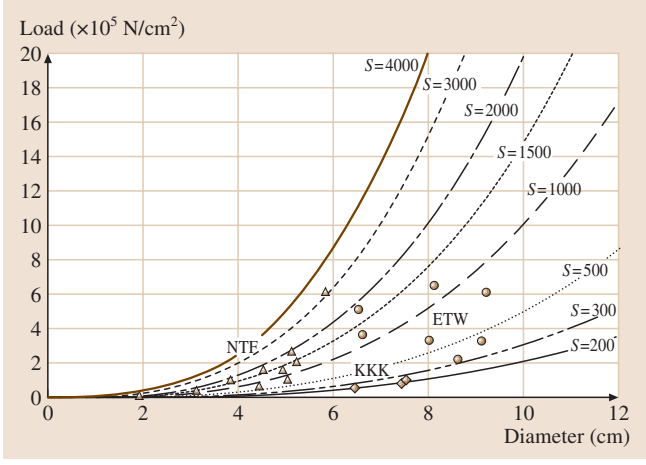

Fig. 8.38 Specific-load parameter of various balances

$$S_\mathrm{rectangular} = \frac{N + L/2 + M}{1,7BH} \,, \qquad (8.32)$$

where L is the active length of the balance without interfaces, D is the diameter, and B and H the maximum available width and height of the balance. The first equation is used when the main cross section of the balance is circular whereas the second one when the main cross section is rectangular. Experience shows that highly loaded balances have a specific load parameter greater than $1000\,\mathrm{N/cm^2}$. In this case the highly stressed areas occur not only in the area where strain gauges are applied, but also in the flexures of the axial force elements.

Bending Section Design. After the distance of the measuring section is fixed, the bending sections must be designed such that the output and full scale are on the order of $0.5\,\mathrm{mV/V}$ to $3\,\mathrm{mV/V}$. The design output depends on the data acquisition equipment to be used. Some systems have a maximum input and therefore it must be guaranteed that no overflow occurs. This is the case even for a single maximum load which can be up to 100% higher than the maximum combined load. In most cases, for maximum output of the design loading, the sum of the full scale output of the force and the full scale output of the moment are the limiting factors. Usually the maximum full scale output is around $1.5\,\mathrm{mV/V}$.

In order to determine the geometry of the bending section it is sufficient to use handbook formulas. If a careful calculation is made the accuracy of the predicted full scale output will be ±10%. Since the real

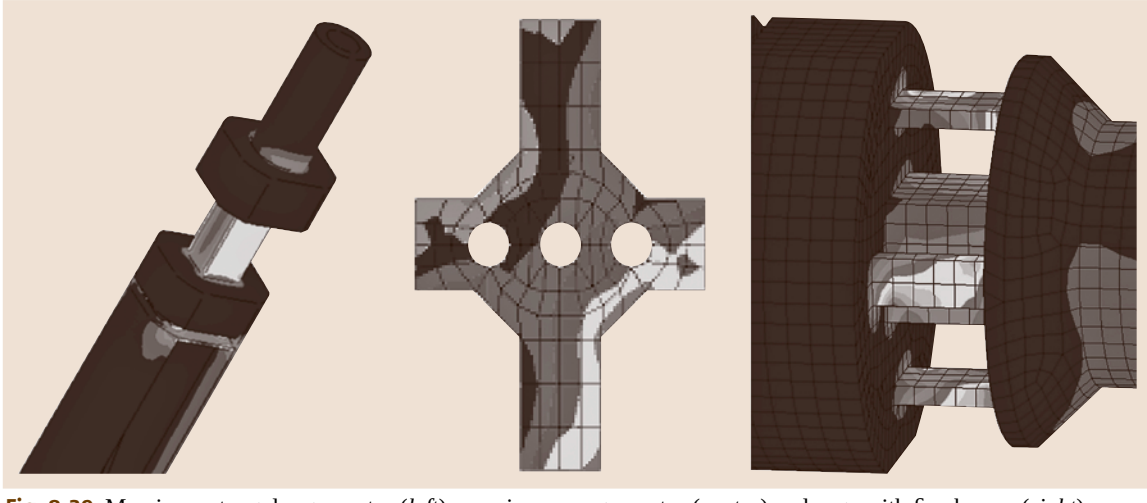

Fig. 8.39 Massive rectangular geometry (*left*), massive cross geometry (*center*) and cage with five beams (*right*)

gauge factor at this stage is not yet known, it is good to use $k = 2$ as default. Normally the real gauge factor is somewhat higher and so the final output of the section is usually higher than calculated.

To design the optimum cross section many different designs are used. Some commonly-used geometries are shown in Fig. 8.39.

Possible Geometries for Bending Section Design. On the surface of the massive cross sections (cross, rectangular or octagonal in shape) the surface stresses caused by the bending moment are measured. In a cage design the tension and compression stresses in the single beams are measured. This design is preferable when the specific load parameter is lower than $300\,\mathrm{N/cm^2}$. During the bending section calculation the measurement sections for five components must be designed. These components are: lift, pitch, side force, yaw and roll.

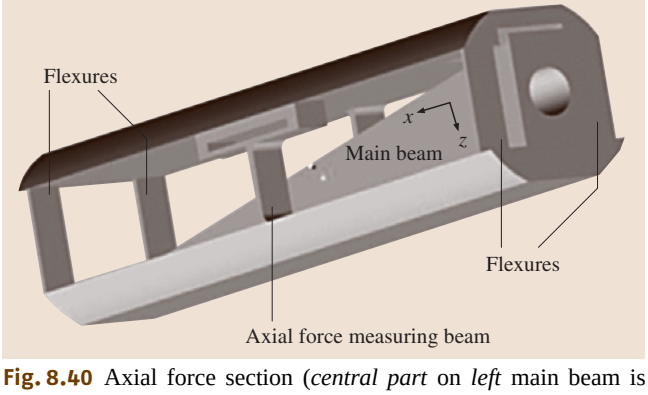

Fig. 8.40 Axial force section (*central part* on *left* main beam is cut out)

Axial Force Section Design. The axial force measurement requires much attention in the design and construction stages. Most of the cost for an internal balance is attributed to the axial force system. Usually the axial force is very small in comparison to the other forces and moments such that the sensitivity of this measurement must be extremely high. This in turn makes the axial force sensitive to interactions of the other components.

In Fig. 8.40 the components of a typical axial force section are shown. The left-hand and right-hand sides of the balance are connected by the flexures. These flexures carry the loads of all five components but are relatively flexible in the axial-force direction. Most of the axial force (more than 60%) is supported by the cantilever beam in the middle of the balance.

The axial force measurements are best made in the middle of the axial force section, since the mechanical interactions are minimal in this position. For thermal effect compensation, in particular temperature gradients, it is better to have four rather than two axial force measuring beams placed near the flexures.

8.1.14 External Balances

Balances have been used since the beginning of aerodynamic testing. One of the first balances ever used was built by *Otto Lilienthal*. In Fig. 8.42 Lilienthal's apparatus for the measurement of lift can be seen. The apparatus

(ΔF_{rm}) is given as:

$$\Delta F_{\mathrm{rm}} = \sum_{i=1}^{n} \frac{\Delta F_{\mathrm{ri}}}{n} \,. \tag{8.37}$$

Subsequently the experimental standard deviation can be calculated from the following equation:

$$S = \sqrt{\frac{\sum_{i=1}^{n} (\Delta F_{\mathrm{ri}})^2}{n-1}} \,. \tag{8.38}$$

The analysis of the residual loads gives the balance user information about the accuracy class of the instrumentation under certain environmental conditions. All the conditions which were kept constant during calibration, like temperature and humidity may have another influence on the accuracy of the measurement in the tunnel itself. Thus the effects of temperature must be corrected or calibrated separately. Another source of error not often taken into account is creep. Creep effects in the balance must be tested separately as well.

All these tests provide information about the accuracy of the balance. However, a few problems remain. Firstly, how to formulate the requirements for the accuracy in a specification? Secondly, how to compare these requirements with the calibration data? One suggestion to solve these problems was made by *Ewald* and *Graewe* in the early 1980's and is briefly described in [8.7]. An equation was formulated that would take into account the error influenced by the number and the magnitude of the interactions:

$$\delta_i = AF_{i\,\max} \left(a_i + b_i \sum_{n=1;n\neq i}^{6} \left| \frac{F_i}{F_{i\,\max}} \right| \right) \,, \tag{8.39}$$

where δ_i is the allowed residual load, $F_{i\,\max}$ is the maximum combined load of component i and F_i the loads applied during calibration. The factor A is the general accuracy factor and the accuracy factor a_i is for the individual component i. b_i is a weighting of the interaction. The customer can specify the factors A, a_i and b_i and after calibration the balance manufacturer has to verify if all the residual loads are below these specifications. A more global verification is to calculate the factors A, a_i and b_i from the calibration data and to compare them with the specifications.

All other influences on the accuracy of a balance can be integrated by using the error propagation law. For the influence of the temperature the (8.39) is rewritten as

$$\delta_i = AF_{i\,\max} \left[\left(a_i + b_i \sum_{n=1;n\neq i}^{6} \left| \frac{F_i}{F_{i\,\max}} \right| \right)^2 c_i^2 + (d_i + \Delta T_1)^2 + (e_i + \Delta T_2)^2 \right]^{\frac{1}{2}} \,. \tag{8.40}$$

Calibration Principles

To obtain the above mentioned data several principles are used during calibration. The first one most used in

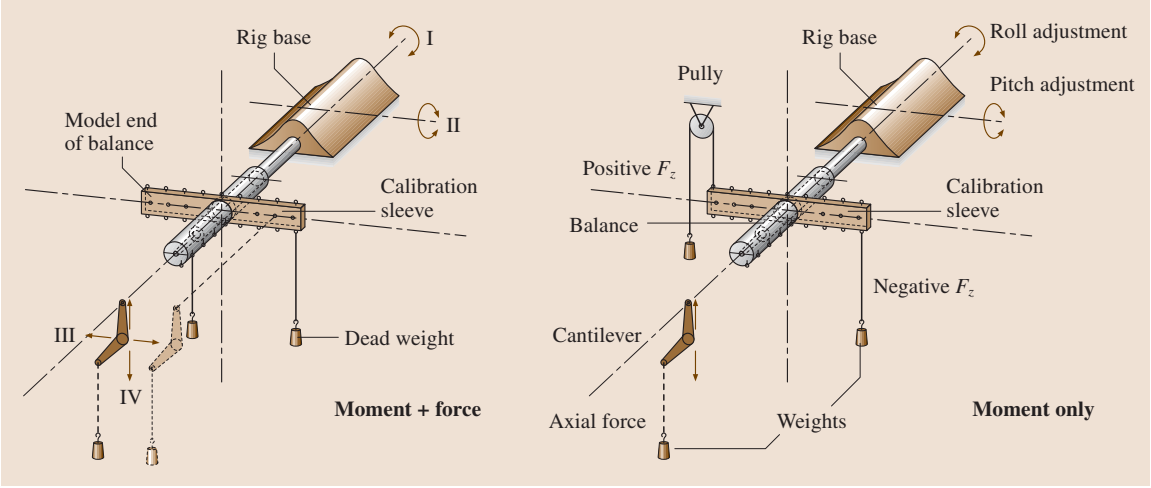

Fig. 8.52 Manual calibration with weights producing: a moment and force (*left*) and a simple moment only (*right*)

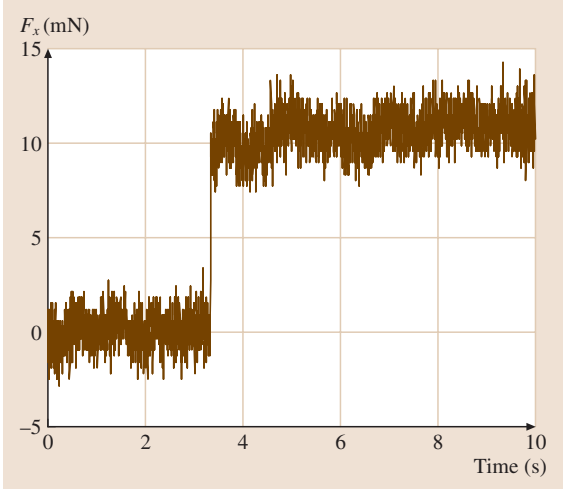

Fig. 8.67 Demonstration of the high resolution of the piezo-balance in its range of highest sensitivity. A 1 g weight was hung from the balance, and then the significant jump was caused by unloading the weight

or a platform balance, which are based on four of the larger transducers (9067). The typical maximum load for each component is at least $F_i \approx 10\,\text{kN}$. Thus, the measuring range extends over six orders of magnitude, since the threshold for dynamic measurements is as low as 0.01 N. Experience shows, as does the later result in Fig. 8.71, that quasistatic measurements are possible down to lower than $F \approx 1\,\text{N}$. Consequently, in the quasistatic mode a measuring range of four orders of magnitude is attainable.

Reproducibility

In order to get a measure for the reproducibility, in a time period of a few hours a calibration cycle was repeated 10 times under normal laboratory conditions. For this test, a platform balance for half-span models was used, based on the larger transducer (type 9067). One calibration cycle was performed with calibration weights of 5, 10, 20, 35 and 50 kg and they lasted roughly 15 min. Table 8.5 shows the results of the measurements. The 2nd column displays the sensitivity of the x-component E_x in [pC/N], determined from the slope of the calibration curves. The 3rd column singles out one measuring point of the calibration cycle, the voltage U_x corresponding to a load of 50 kg.

Calculating the mean and the standard deviation we find for the sensitivity of the x-component:

$$E_x = (7.8634 \pm 0.0005)\,\text{pC/N}\,. \tag{8.42}$$

Table 8.5 Results of 10 calibration cycles repeated under normal laboratory conditions

Cycle No	E_x (pC/N)	U_x (V/50 kg)
1.	7.8637	1.9287
2.	7.8638	1.9287
3.	7.8625	1.9283 min
4.	7.8634	1.9285
5.	7.8630	1.9285
6.	7.8633	1.9284
7.	7.8632	1.9285
8.	7.8631	1.9285
9.	7.8644	1.9288 max
10.	7.8636	1.9285
Mean	7.8634	1.9285
Stand. dev.	0.0005	0.0002

The ratio between the difference of the peak values and the full scale range can be seen as a measure of the reproducibility. These values can be derived from the 2nd column: largest deviation $U' = U_{x\max} - U_{x\min} = 0.5\,\text{mV}$, full-scale range $(x_{12} + x_{34})$ each 10 V $\Rightarrow U_{\text{FS}} = 20\,\text{V}$.

Thus the reproducibility has a value of:

$$\frac{U'}{U_{\text{FS}}} = 0.025‰\,. \tag{8.43}$$

These results are also, at least, representative for the other external balances and they demonstrate that it is possible to attain good accuracy if one is able to hold the ambient conditions constant.

Behaviour Under Cryogenic Conditions

As mentioned in the introduction, a piezoelectric balance was built for the cryogenic Ludwieg tube in Göttingen (KRG) in such a way that the balance itself is totally in the cryogenic environment. This fact is not self-evident as such a balance has to withstand a large amount of thermal stresses when the temperature is changed over the entire range of the cryogenic facility.

To clear up the question as to the extent the force measurements can be made with piezoelectric transducers at cryogenic conditions was one motivation for this activity.

At our request, a special version of transducer type 9252 was manufactured by Kistler for application at cryogenic temperatures. The modification concerns the insulators in the plugs by default made from silicone, which were replaced by ceramic ones such that application down to cryogenic temperatures ($T = -150°$) and pressures up to 10 bar was more feasible. The modifi-

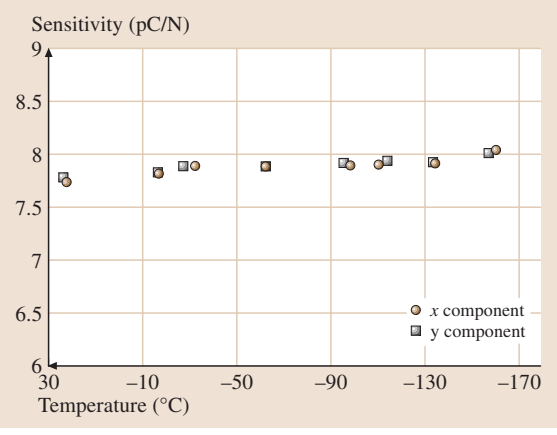

Fig. 8.68 Determination of the sensitivity of the shear components F_x and F_y of the cryo-balance depending on temperature

cation mainly ensures that no humidity effects diffuse in the transducer case during the unavoidable large temperature changes.

Before application in the windtunnel, the balance with the modified multicomponent transducers (Sect. 8.2.1) was tested and calibrated in a cryostat down to a temperature of $T = -160°$. The low temperature was produced by injection of vaporised nitrogen. For the connection between the force transducer in the cryostat and the charge amplifier outside, the usual cables for piezoelectric sensors could be used.

In the pre-tests we found no significant deviation in the behaviour of the balance compared with normal conditions concerning drift or electrical noise of the signals.

The calibration was conducted using weights, which were appended outside of the cryostat via cables. Concerning the axial component F_z, it was found that the cool-down from 24° to −169° led to a contraction of the prestressing bolts resulting in 1.5 kN increase of the prestressing force, which is one order of magnitude smaller than the standard prestress. This effect was caused by the different thermal expansion coefficients of the transducer and the prestressing bolt.

Both shear components F_x and F_y showed good linearity compared to that at normal conditions, and the slopes i. e. the sensitivities, dependent on temperature are displayed in Fig. 8.68. It is obvious that the sensitivity slightly changes with temperature. This sensitivity shift is caused by the fact that the corresponding piezoelectric coefficient (d_{11}), which is responsible for the shear effect, is slightly increasing with decreasing temperature [8.17].

In this context, it should be mentioned that at normal conditions, arrangements of force transducer are also sensitive to temperature changes during a measurement cycle. This problem concerns, in particular, the direction of the prestressing bolts. Thus, in any case the balances must be protected against changes in the thermal distribution, at least while a running measurement.

Measuring Time for Quasistatic Measurements

As mentioned, the piezoelectric measuring system is an active one, which generates an electrical quantity. Herein lies a fundamental disadvantage, namely that only quasistatic measurements are possible. A time constant $T = R_g C_g$, characteristic for the exponential decline of the charge signal, results from the entire input capacity C_g and the finite insulation resistance R_g, posed by the transducer, cord, plugs and amplifier input etc. Further fault currents in the charge amplifier, which are fortunately independent from the load, cause the zero-point to drift. Thus the combined error is smaller, the larger the charge on the quartz, meaning that the effective measuring time increases as the loading and the sensitivity increase. Fortunately, the drift is dominated by the fault currents in the input devices of the charge amplifier, which are nearly constant, leading to a linear drift depending on time at the output. The sign of the drift can be positive or negative. A simple linear correction for every test point in time can be computed as follows: For each measurement, the raw data, integrated in time, and the corresponding time are stored. Knowing the zero point before the measurement (flow speed $U = 0$) and after the measurement (where the flow speed is zero again), a correction can be computed by linear interpolation.

In order to give an impression on the drift behaviour under nearly extreme conditions, the time function of the 3 components of the cryo-balance were recorded, while the balance was attached to the calibration setup, i. e. without load and under good environmental laboratory conditions. In addition, the cables and plugs were verified to have an overall resistance of at least $R \approx 10^{13}\,\Omega$. In another (unfavourable) condition, the system was switched in the range of highest sensitivity, where the drift effect was maximal. Figure 8.69 shows first, that the drift was rather linear for all three components and secondly, that at least at good environmental conditions the drift effects are not as extensive as generally believed. In other words, the results show the probable lower reachable limit when the compo-

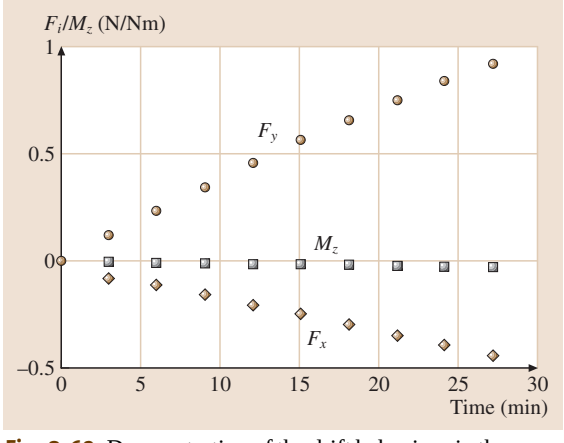

Fig. 8.69 Demonstration of the drift behaviour in the range of highest sensitivity of the entire force measuring system under ideal environmental conditions

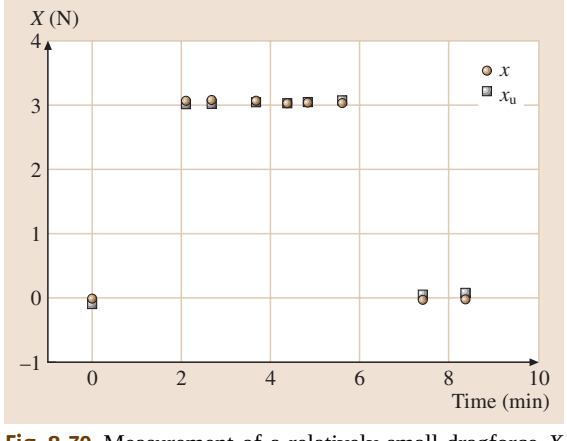

Fig. 8.70 Measurement of a relatively small dragforce X on a building model, taken in the boundary layer wind tunnel of the University of Florence using the cryo-balance ($u = \text{const} = 4.3\,\text{m/s}$. wind off at $t = 0$ and $t > 7\,\text{m}$). X_u: uncorrected values i. e., without drift correction

nents such as plugs, cables etc. are selected and the test conditions are nearly optimal.

In order to provide an impression of the drift error at small loads, an example is presented in Fig. 8.70, taken in the boundary layer windtunnel of the University of Florence. A simplified building model was mounted at the cryo-balance corresponding to the sketch in Fig. 8.58. The figure shows a measurement of a relatively small drag force of $X = 3.1\,\text{N}$ at a low flow speed $u = \text{const} = 4.3\,\text{m/s}$ dependent on time t. The airflow was started at $t = 0\,\text{min}$ and switched off for $t > 7\,\text{min}$. The index u (X_u) denotes values without drift correction. Looking at the + symbol(uncorrected) at $t = 0\,\text{min}$, we see a small deviation in negative direction, caused by switching on to the operate mode. At the end of the measurement run at $t = 8.5\,\text{min}$, there is also a small deviation but in positive direction. The small difference in the outputs between start and end is caused by the drift in positive direction. After correction, the corresponding points (symbol $_*$) lie on the zero line.

Although the windtunnel speed is not exactly constant, we can state that the effect of the drift of the zero-point is not as extensive as generally believed.

8.2.3 Examples of Application

Bluff Bodies in a High-Pressure Windtunnel

The flow around a circular cylinder is a classical problem of fluid dynamics, which exhibits strong Reynolds number effects mirrored in drastic variation of the drag coefficient and Strouhal number. A second classical bluff body case is the sharp edged, square section cylinder, which has a high drag coefficient nearly independent of the Reynolds number.

Thus, both sections were selected as examples concerning force measurements performed in the high-pressure windtunnel (HDG). The flow speed ranged from 2 m/s to 38 m/s, the pressure could be increased up to 100 bar and the test section measures $0.6 \times 0.6\,\text{m}^2$. Since even steady loads in this low-speed wind tunnel can vary over four orders of magnitude merely by changing the flow parameters, the results give an impression of the large dynamic range of a piezo balance. Indeed, this property of the wind tunnel and the deduced requirement of a large dynamic range motivated the author to design and built his first piezo balance [8.**?**].

The principle setup of the balance was described in Sect. 8.2.1 (Fig. 8.63). We selected the larger 3-component force measuring elements (Kistler, type 9067), because of their large load range. A special difficulty when measuring in the high-pressure windtunnel is the fact that the model, the sensors and the balance are located in the high pressure section, where it is desirable to have the electronic equipment outside at atmospheric pressure. Since one of the primary prerequisites for quasistatic measurements is that an insulation resistance of $R \approx 10^{13}\,\Omega$ is reached for all connections between the force element and charge amplifier, a special solution was necessary for the crossover from the high to the atmospheric pressure section. Because this requirement is difficult to satisfy with hermetic connectors, the necessary cables were inserted into flexible pressure-

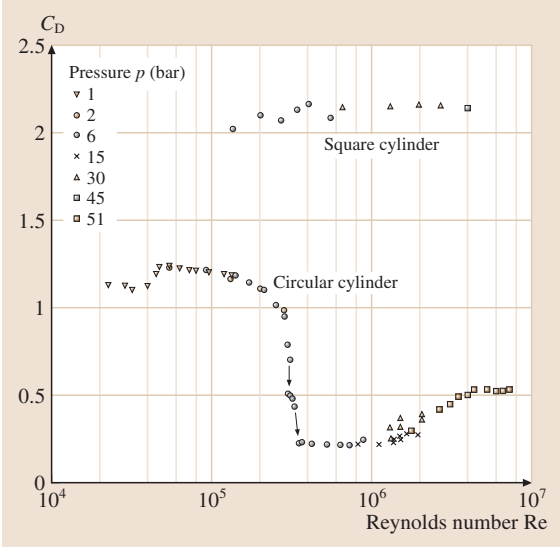

Fig. 8.71 Measurement of drag coefficients of a circular- and a square cylinder in the high-pressure windtunnel. Due to the large dynamic range of the balance the individual Re number range could be overlapped by merely changing the flow parameters

resistant hoses, which were pressure sealed connected at the transducer and then laid out through the windtunnel wall and connected to the charge amplifier outside of the high pressure section. In this way, atmospheric pressure was maintained within the element, as well as in the corrugated hoses, so that an increase of static pressure in the windtunnel acts as a preload on the element. Since the zero-point in the sensor/charge-amplifier system can be chosen arbitrarily by short-circuiting the charge, the preload in axial direction has no significant influence on the accuracy of the measurement.

This modification of the force transducer for application at high pressure up to 100 bar was also manufactured by Kistler.

Such modified transducers were also applied in several water tanks in Hamburg to measure the forces on ship models and marine structures [HSVA Jochmann]. A detailed description of the balance and many results concerning flow around more or less bluff bodies can be found in [8.10, 11, 18–20].

As an example of a quasisteady measurement, Fig. 8.71 shows drag coefficients of a circular cylinder and a square cylinder dependent on the Reynolds number. The flow speed was increased up to 40 m/s and the pressure up to 51 bar. In the case of the circular cylinder, the smallest drag force was 0.8 N at the lowest Reynolds number. The largest drag force was about 2000 N for the square cylinder at Re $\approx 5 \times 10^6$. Since only about 20% of the range of the balance was used, it was demonstrated that, in principal, steady measurement over four orders of magnitude was possible. As for fluctuating forces, the dynamic range is extended to six orders of magnitude because the resolution is about 0.01 N.

Figure 8.72 depicts a typical dynamic measurement, which is representative of the ability to resolve and detect even very weak nonlinear effects in a global force measurement. The figure shows the power spectra of the lift – and drag fluctuations on a square cylinder at an angle of incidence of $\alpha = 10°$. In this state, the free separated shear layer is probably more or less regularly attaching to the side wall of the square cylinder producing sub- and superharmonic peaks. It is surprising that this localised effect can be found and resolved in a global, i. e.integrated measurement. In addition, apart from the fundamental Strouhal peak and the sub- and superharmonics, there are significant peaks at 3/2 and 5/2 of the vortex shedding frequency [8.21]. The dynamic is reflected in the distance between the spectral densities, which is up to 50 dB.

Further applications concerning force measurement on a bridge section and an airfoil at high angle of attack can be found in *Schewe* [8.19].

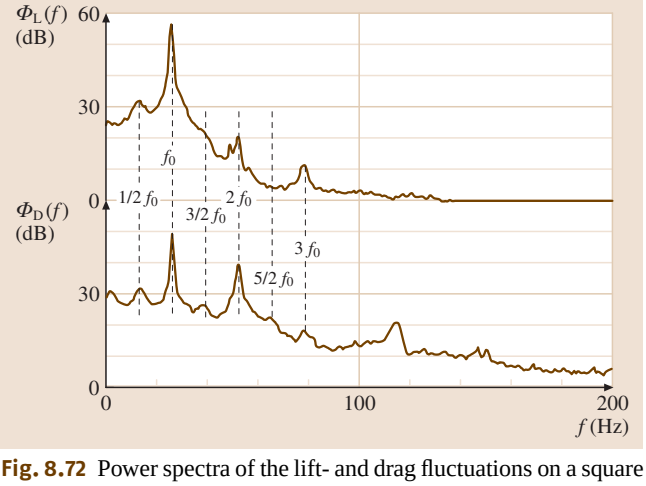

Fig. 8.72 Power spectra of the lift- and drag fluctuations on a square cylinder at an angle of incidence of $\alpha = 10°$. Even the very low intense sub- and superharmonics can be resolved. The distance of the peak height is up to 50 dB

Typical Half-Span Model in a Conventional Low-Speed Windtunnel

The wing/engine combination described in Sect. 8.2.1 was tested in the low-speed windtunnel ($3 \times 3\,m^2$) in Göttingen. The project comprised force and pressure distribution measurements. The influence of the thrust of the ejector engine on the aeroelastic and aerodynamic behaviour of the wing/engine combination was of particular interest. For this reason, in the engine model four multicomponent force transducer were installed to measure separately the global forces on the engine. More about the motivation for the project, a detailed description of the test setup", and the results of the pressure measurements can be found in *Triebstein* et al. [8.15].

Figure 8.73 shows as an example the steady normal force and its rms value for angles from $-4°$ up to $14°$, taken at a flow speed of 60 m/s. In this case the balance was not fixed to the windtunnel, but rotated with the model, thus the normal force on the wing and not the lift was measured. The results demonstrate that the measurement of steady forces is possible with sufficient accuracy. The angle $\alpha = 0$ was measured twice – at the beginning and at the end of the test run. Within drawing accuracy, both measuring points overlap.

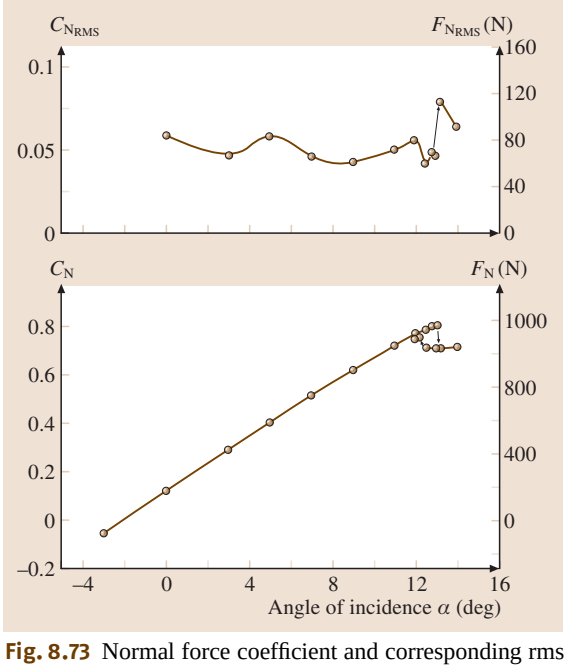

Fig. 8.73 Normal force coefficient and corresponding rms value depending on angle of incidence of a wing/engine combination in a low-speed windtunnel. C_N (α) is not a straight line since the balance is rotated with the wing. After the discontinuous drop of the steady normal force at 13°, the rms jumps to nearly double its previous value

Referring to the span of the measurement range, it should be mentioned that at the maximum normal force of more than 1000 N, the range of the balance is used by only about 6%, meaning that this balance can also be applied at much higher loads (i. e. in the transonic range without any changes being necessary.

As an example for an unsteady measurement, in the upper part of the Fig. 8.73 the rms of the normal force is presented, which is nearly constant below the onset of flow separation. After the discontinuous drop of the steady normal force at 13°, the rms jumps to nearly double its previous value. One has to bear in mind that inertia forces are included.

The rms of the bending moment was also measured, and it has similar behaviour. All rms values were obtained by integrating the corresponding power spectra. Figure 8.74 shows two examples of normal force spectra, immediately before and at the onset of the flow separation. The dotted line represents the spectrum taken at $\alpha = 13.2°$, the solid line the spectrum taken at 13°. The spectra are dominated by a rather narrow peak at the bending frequency of the wing. The bending frequency is excited by the noise-like random contributions which are inherent in the flow. Particularly after the onset of the flow separation, the intensity of the fluctuating aerodynamic loads and, consequently, the bending vibration of the wing increase drastically. Hence, the rms jumps to nearly double its previous value in the normal force and bending moment. When considering these unsteady

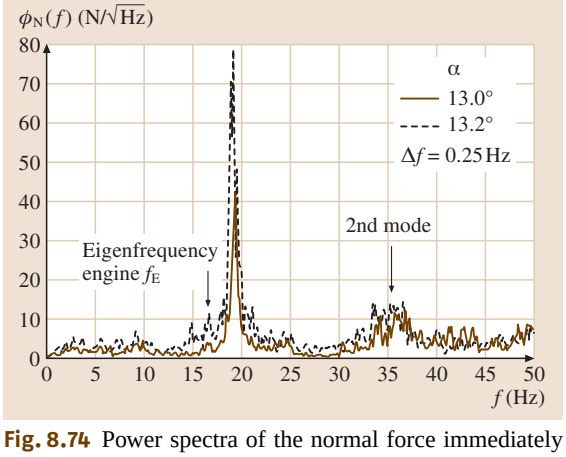

Fig. 8.74 Power spectra of the normal force immediately before ($\alpha = 13°$) and at the onset ($\alpha = 13.2°$) of the flow separation. Concerning the balance, there are no resonance peaks caused by the force measuring system itself

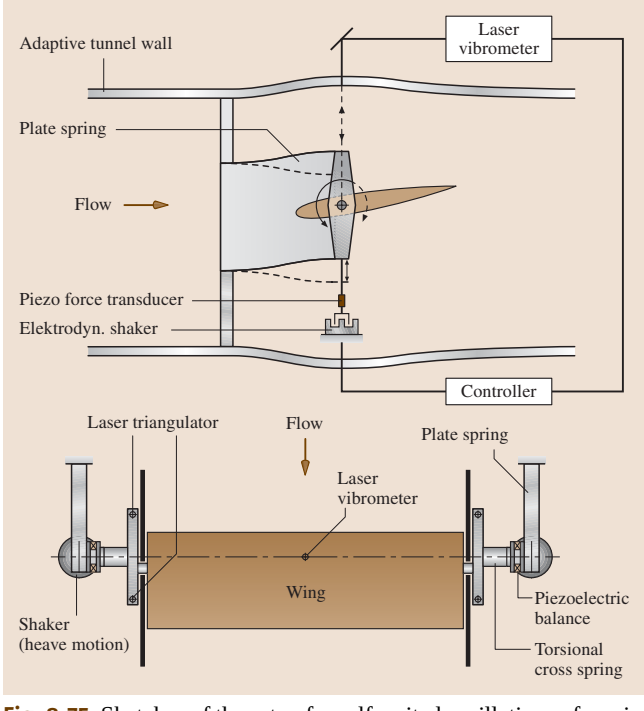

Fig. 8.75 Sketches of the setup for selfexcited oscillations of an airfoil in two degrees of freedom. A piezoelectric balance is installed on each side between the bending and the torsion spring. A laservibrometer, the electrodynamic exciter and the controller form the flutter control system. The exciter force is also measured using piezoelectric force transducers

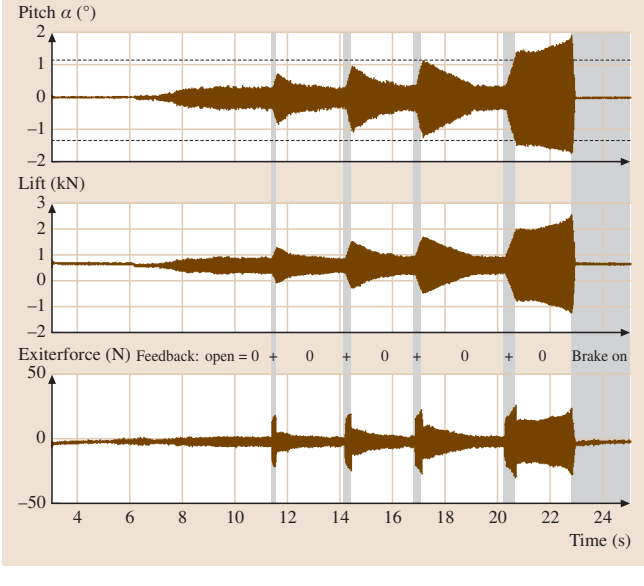

force measurements, it is important to remember that the signals contain several components. In addition to the aerodynamic loadings, contributions of elastic and inertia forces due to the vibration are also present.

Finally, it can be stated that the changes of the flow field at the onset of separation lead to a small frequency shift of the bending frequency. This frequency change, Δf, represents a small contribution to the stiffness, caused by aerodynamic effects.

As for the balance, the spectrum shows that there are no significant peaks which could be produced by the balance itself.

Aeroelastic Experiments: Oscillating Models in a Transonic Windtunnel

Aeroelasticity studies the interplay between elastic structures in an air stream and its aerodynamic forces and moments. The interaction between aerodynamic and structural forces may lead to complicated nonlinear static and dynamic effects, for example the feared flutter oscillations. Thus knowledge of the steady and unsteady forces and moments is very essential. Therefore three different setups for aeroelastic experiments at airspeeds up to the transonic regime have been developed. These setups are usually applied in the $1\,\mathrm{m} \times 1\,\mathrm{m}$ adaptive test section of the transonic windtunnel in Göttingen.

The first setup sketched in Fig. 8.75 is designed for investigating flutter phenomena of airfoil models. It is symmetrically built from blade- and cross-springs for a bilateral elastic suspension. To measure the steady and unsteady forces, a piezoelectric balance is installed on each side between the bending and the torsion spring. Each balance corresponds to the platform balances comprising four multicomponent elements (type 9252) as described for half models in Sect. 8.2.1. In case of flutter or forced motion the balance is oscillating in heaving direction. Therefore the smaller transducers were selected due to their lower weight and the advantage gained by reducing the moving masses.

Figure 8.75 also shows a schematic representation of the flutter-control system used to dampen or excite oscillations of the model. A laser vibrometer was used to measure heaving motion of the airfoil oscillations.

Fig. 8.76 Artificial initiation of selfexcited flutter oscillations in a hysterisis regime (subcritical bifurcation). The initial amplitudes are set for different temporal lengths via positive feedback. The limit amplitude of $\alpha = 1.2°$ acts as a repeller. Depending on whether or not the initial amplitudes lie below or above this threshold value, the oscillations will be damped or excited

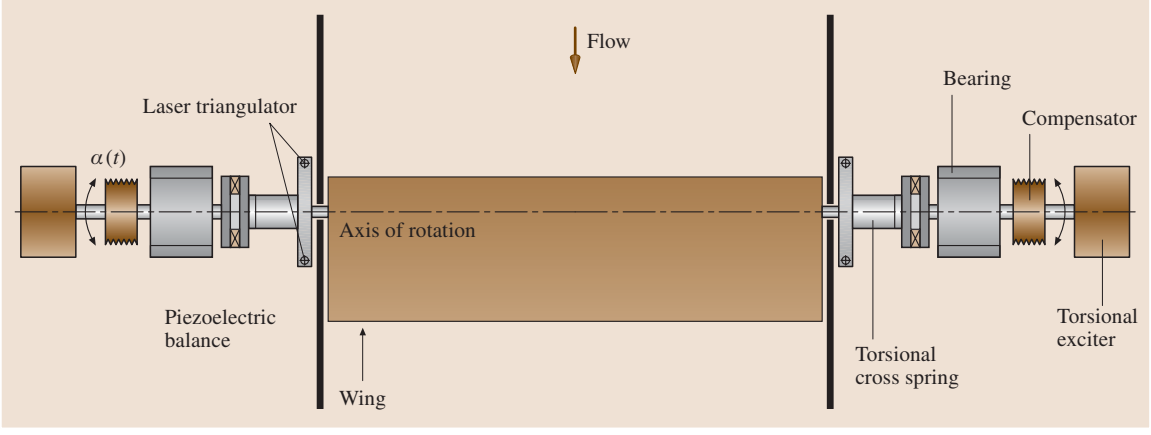

Fig. 8.77 Pitch test setup for forced torsion oscillations. The installation of both optional torsion springs (cross springs) gives the wing a torsion degree of freedom for investigating torsional flutter. The piezoelectric balances are between the hydraulic actuators and cross springs

The heave-speed signals were fed into an operational amplifier and then into one electrodynamic exciter at each side. The excitation is acting directly on the bending springs in heave direction, whose connecting box forms the basis for the piezoelectric balance. Thus the excitation forces do not act directly on the piezoelectric balance, but rather appear only indirectly in the balance signals since the heave motion of the airfoil induces inertial forces. Forced heave oscillations can be driven by replacing the electrodynamic exciters by stronger hydraulic linear actuators. The exciter force F_{ex} itself can be measured directly with the one component piezoelectric force sensor (Kistler 9301 A), built into the heave rod.

Figure 8.76 shows an instructive example of a flutter measurement using a symmetrical NACA 0012 airfoil taken at the flutter boundary. The state of the system is critical i. e. in the transition range between stability and instability. We will see that it is a hysteretic-encumbered transition (subcritical bifurcation), which was recorded at a mean angle of attack of $\alpha = 1.1°$. The curves plotted in the Fig. 8.76 are for (a) the angle of attack $\alpha(t) - \alpha_{mean}$, (b) the lift force $L(t)$, and (c) the heave-rod force F_{ex} of the excitation, measured with the piezoelectric transducer. First we see in the offset that the mean lift is 0.7 kN. Second the time functions demonstrate how the system reacts to disturbances of different strengths or durations. Such a disturbance occurred when the control device was switched to positive feedback for a short time. The period of excitation of the system can be clearly seen in the curve for $F_{ex}(t)$, where the amplitudes shoot up at the indicated time points at $t \cong 11.3$, 14.2, 16.5, and 20.0 s. It is also obvious that the time span of the disturbances increases with increasing time. Whereas the flutter oscillations decay after the first three short bursts of excitation, they diverge after the fourth, the longest of the excitations. This behaviour indicates that we must be in the hysteresis range of a subcritical bifurcation, i. e., the last disturbance was sufficient to lift the system above an unstable limit cycle, which then acted as a repeller to cause the increase in the amplitudes. At this point, we should note that the forces needed to influence the system are about two orders of magnitude smaller than the lift forces that occur, even though $F_z(c)$ still contains inertial forces.

Finally the example shows that it is possible to perform measurement of steady and unsteady forces under very difficult conditions, i. e. while the balance is oscillating.

By use of the second test setup (Fig. 8.77), the aerodynamic effect of forced pitching motions of a model may be investigated. In this case, two torsional hydraulic actuators work with 180° phase shift and force the pitching motion of a two-side suspended model in the air stream. It is successfully used for example in testing airfoil models equipped with piezoelectrically driven flaps for dynamic stall control. The piezoelectric actuators use the inverse piezoelectric effect and are described by *Schimke* et al. [8.22]. This test setup can be upgraded with a torsional degree of freedom in order to investigate free pitch oscillations of the model. To measure the steady and unsteady forces, the same piezoelectric balances described above can be installed on each side between the hydraulic

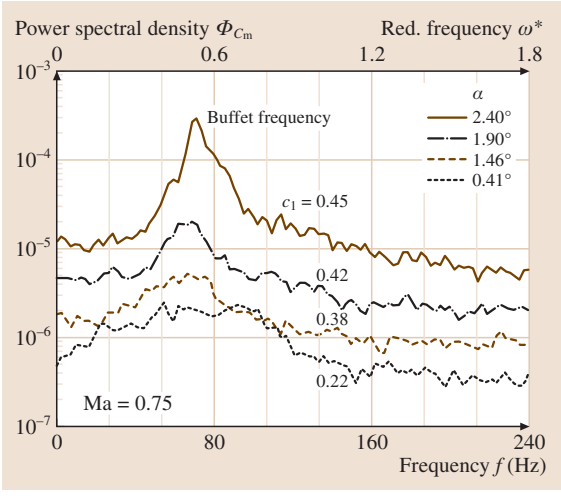

Fig. 8.78 Power spectra of moment fluctuations for different angles of attack for a fixed supercritical airfoil. With increasing α a peak at the buffet frequency of $\omega* = 0.56$ shows up. The corresponding steady lift coefficients c_l are also included

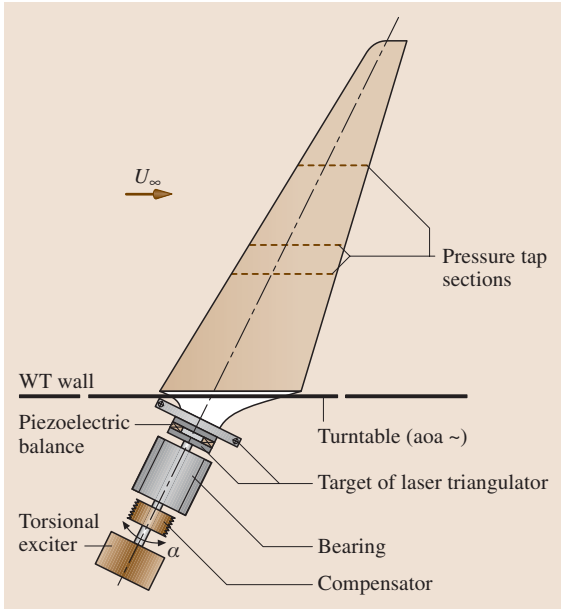

Fig. 8.79 Test setup for oscillating half models in the transonic windtunnel. The piezo balance is located at the root of the wing

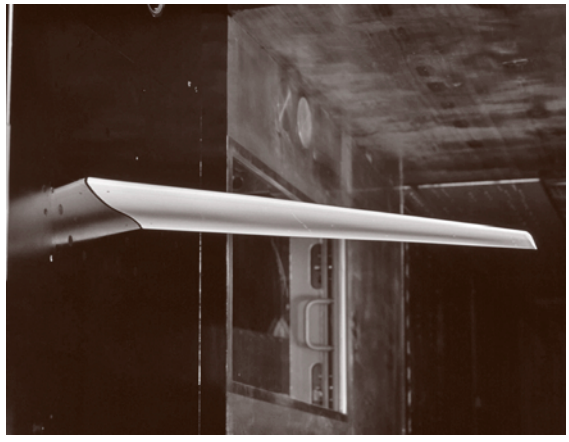

Fig. 8.80 Elastic wing models in the adaptive test section of the transonic wind tunnel

actuators, the model, and the optional crossprings, respectively.

The ability to investigate unsteady phenomena like buffet oscillations in transonic flow is demonstrated in Fig. 8.78 where spectra of the moment fluctuations are presented. In this case, the crossprings were not installed, the model with supercritical section (NLR 7301) was at rest, and the angle of incidence α was varied using the hydraulic actuators.

These spectra show what happens when α is increased while the Mach number is held constant at Ma = 0.75. Above an angle of attack of $\alpha = 1.5°$, there appear peaks in the spectra that can be traced back to selfexcited shock oscillations (buffet) and, therefore, because of the absence of the necessary degrees of freedom for oscillations, have purely fluid-dynamical origins. The non-dimensional buffet frequency has a value of $\omega* = 0.55$, which corresponds to a frequency of $f = 72.7$ Hz. Simultaneously, the mean lift was measured and the values are included in the figure. For this type of measurement, the high stiffness of the twin sided piezo-balance is a significant prerequisite. The test setups and the experiments are described in more detail by *Schewe* et al. [8.23].

The third test-setup, sketched in Fig. 8.79, shows that a wing model is mounted on a turntable device such that the wing meets the sidewall with a negligible gap. The turntable device allows adjusting the model's angle of attack around an axis perpendicular to the sidewall of the test section. Furthermore, the model can be forced by means of a hydraulic rotation actuator to perform pitch oscillations around the spar axis plotted in Fig. 8.79. Laser triangulators are used to measure the pitch according to the spar axis. Also here, a piezoelectric platform balance is used to measure the root loads outside of the test section. The time-averaged signal of the balance al-

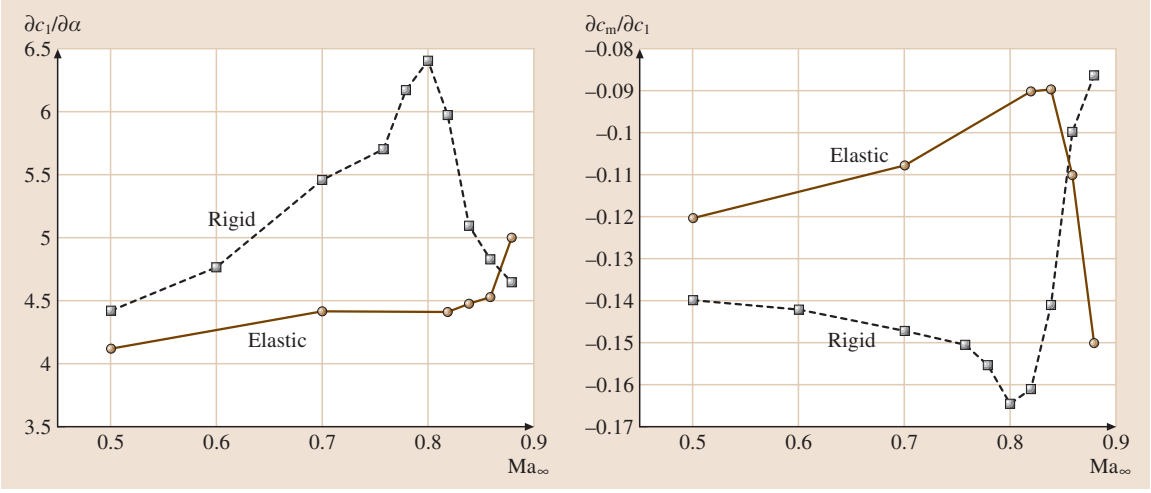

Fig. 8.81 Comparison of the lift-curve slope $\partial c_l/\partial\alpha$ and $\partial c_m/\partial c_l$ for the rigid and the elastic model upon the Mach number

lows determining the global aerodynamic loads, while the unsteady part of the balance signal represents the sum of unsteady air loads and inertia forces.

Figure 8.80 shows the half-spanmodel of the project "Aerostabil" [8.24] mounted in the adaptive testsection of the Transonic Windtunnel Göttingen (TWG). There are two models with the same outer geometry, representing the outer part of a transport aircraft wing with a supercritical airfoil section. The first model was designed conventional, i. e. as rigid as possible and the second was elastically scaled corresponding to the prototype. The aim was to study the static aeroelastic effects,

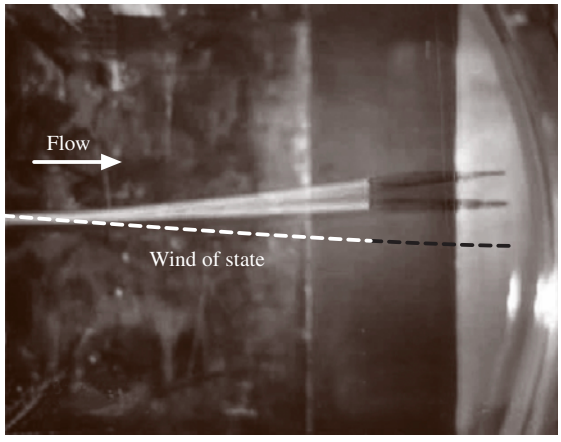

Fig. 8.82 Half-span model twisted and bended by air loads in the state of a limit cycle oscillation (LCO). Such measurements postulate a rigid balance

which were often ignored in the past. Figure 8.81 shows the influence of the elasticity of the swept wing for the dependence of the lift curve slope $\partial C_L/\partial\alpha$ and the pitching-moment-slope curve upon the Mach number at a constant angle of incidence at the model root and constant Reynolds number. Significant differences due to elastic deformation can be seen as the lift curve slope is reduced up to 16% at $Ma = 0.83$. For the highest Mach numbers, the regions on the wing with flow separation are probably larger in the case of the rigid model resulting in smaller values of the lift curve slope.

If the elasticity of a half-span model is designed in an appropriate way, flutter tests can be performed in this test setup as can be seen in Fig. 8.82. We see a snapshot of the half wing twisted and bended by the steady air loads, in addition the wing is undergoing flutter i. e. a limit-cycle oscillation (LCO) at a Mach No. of $Ma = 0.865$.

Circular Cylinder in a Cryogenic-Ludwieg-Tube

The flow around a circular cylinder and its dependence on the Reynolds number is one of the most important problems and favourite test cases in fluid dynamics. Thus, this simple geometry was selected for the first application of the piezoelectric balance under cryogenic conditions [8.25].

The measurements were performed in the cryogenic Ludwieg tube in Göttingen (KRG), which is a blow-down windtunnel for high Reynolds number research in transonic flow and is described by *Rosemann* [8.26]. The Mach number range is $0.28 < Ma < 0.95$ and high Reynolds numbers up to more than 10^7 are achieved by

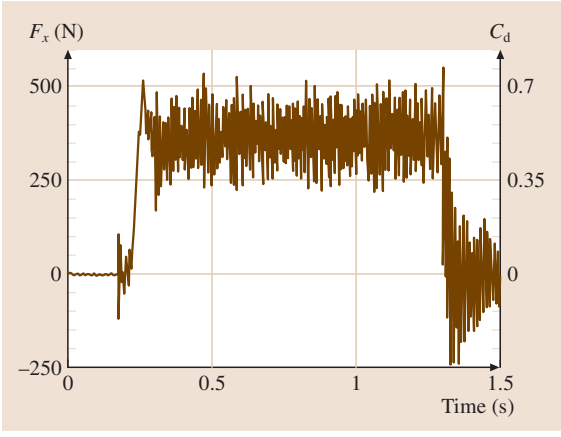

Fig. 8.83 Drag depending on time for a circular cylinder, measured with a piezo-balance in the cryogenic Ludwieg tube at extreme conditions ($\mathrm{Re} = 5.8 \times 10^6$, $\mathrm{Ma} = 0.28$, $T = -150°C$, $p_0 = 10$ bar). The drag coefficient is $c_d = 0.53$, taken in the time window Δt between 0.8 and 0.9 s

cooling down the fluid medium to nitrogen temperature and by pressurizing up to 10 bar. The test section measures $0.4 \times 0.35\,\mathrm{m}^2$ and the effective measuring time is roughly 0.5 s.

The test setup is similar to the others using two-dimensional models such as airfoils or cylinders. Behind each wall of the rectangular test section there is a cryo platform balance, attached to a solid base at the test section. Similar to the high pressure windtunnel, the circular ends of the freely suspended circular cylinder are passed through the windtunnel walls and the ends are clamped in the holes of the force conducting top plate of each balance by a ring locking assembly. In this case, both balances can also be connected in parallel, thus electrically they are acting as one balance yielding three signals for drag, lift and moment.

Figure 8.83 shows a typical result for the drag force as a function of time, measured on a smooth circular cylinder (aspect ratio = 11.4) at extreme values of the operating range of the facility. The intention was to get the highest possible Reynolds number in nearly incompressible flow. Thus the measurement was taken at the lowest temperature of $T = -150\,°\mathrm{C}$, the highest pressure possible $p_0 = 10$ bar and the lowest attainable Mach number of $\mathrm{Ma} = 0.28$, resulting in a Reynolds number of $\mathrm{Re} = 5.8 \times 10^6$. The curve clearly shows that with the onset of flow, the drag increases rapidly up to a certain level, remains there as long as flow continues, then decreases quickly to zero when flow ceases. The drag coefficient is $c_d = 0.53$, and a narrow peak in the spectrum of the lift fluctuations (Fig. 8.84) generated by the Karman vortex street, leads to a Strouhal number $\mathrm{St} = 0.25$. In order to substantiate the force measurements, pressure measurements at the shoulder of the cylinder ($\varphi = 90°$) were performed with a pressure sensor (Kulite). The lower spectrum in Fig. 8.84 displays the behaviour of the fluctuating pressure and thus confirms that the corresponding peak in the force spectrum is indeed due to the Karman vortex street at the same Strouhal number.

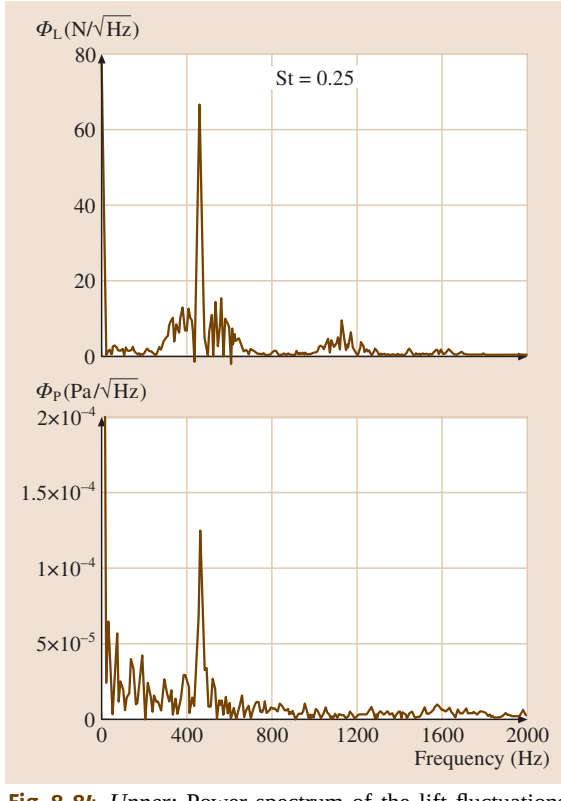

Fig. 8.84 *Upper*: Power spectrum of the lift fluctuations corresponding to above measurement. *Lower*: Power spectrum of the pressure fluctuations at the shoulder of the circular cylinder ($\varphi = 90°$)

The rms-value of the lift fluctuations for this case amounts to $c_1' = 0.20$, which is more than double the value as in other measurements [8.10].

The reason is the fact that at the lowest Mach number and with that low flow velocity the also low vortex shedding frequency ($f_V = 465$ Hz) was quite near the natural frequency of the cylinder ($f_n = 435$ Hz) leading to superelevation due to resonance effects.

The measured drag coefficient and the Strouhal number are in good agreement with the result in the high pressure wind tunnel [8.10].

The strong oscillations in the drag signal, in particular after the flow has ceased ($t > 1.3$ s) can have many causes. One could be the mentioned proximity to the vortex resonance range.. Although the vortex induced drag fluctuations have double the value of f_{Vortex}, a higher order resonance due to nonlinear interaction may be responsible for the significant oscillations in the drag signal. In any case the rapid decrease of the flow velocity acts as a transient or jump excitation on the cylinder. This effect was not observed when both frequencies were well separated.

Nevertheless, it is interesting to note that, in spite of the pulse operating mode of the tunnel, the steady and unsteady processes can be measured very well.

8.2.4 Conclusions

Based on the applications described before, the typical positive properties of a piezo balance can be summarized as follows:

- High rigidity, which leads to small static deformations and to high natural frequencies
- Low interferences, which are typically lower than 1%
- High resolution (< 0.01 N), which is independent on the preload
- A large dynamic range; dynamic: 6 orders of magnitude, quasistatic: up to 4 orders of magnitude possible
- Application in difficult ambience possible such as cryogenic conditions, very high pressure and water.

Properties of piezoelectric measuring systems, which can be disadvantageous, when the generated charges are small:

- Restricted to quasistatic measurements imposed by the drift of the zero point, but this is not as extensive as generally believed and drift corrections are possible.
- Sensitivity to temperature changes during the measurement in particular in direction of the prestressing bolts

Finally, in the field of aircraft aerodynamics, when the flow is attached and the interest is focused on drag measurements with a resolution of drag counts ($\Delta C_{\text{d}} = 0.0001$) the application of strain gauge balances is suggested, since so far a piezoelectric measuring system cannot guarantee accuracy for very small steady values.

In all problems, where the flow is more or less separated, for example in bluff body flows or situations around stall or when the model is oscillating, a high end drag measurement has less significance and the disadvantages of piezo balances are more than outweighed by its inherent rigidity with the known positive consequences.

References

8.1 ISO: *Guide to the Expression of Uncertainties in Measurements* (International Organization for Standardization, Geneva 1995)

8.2 AIAA: *Assessment of Experimental Uncertainty with Application to Wind Tunnel Testing, AIAA S-071A-1999* (AIAA, Reston 1999)

8.3 AIAA: *Calibration and Use of Internal Strain Gauge Balances with Application to Wind Tunnel Testing, AIAA R-091-2003* (AIAA, Reston 2003)

8.4 B. Ewald, G. Krenz: *The accuracy problem of airplane development force testing in cryogenic wind tunnels, AIAA Paper 86-0776, Aerodynamic Testing Conference Palm Beach* (AIAA, 1986)

8.5 B. Ewald: *Balance Accuracy and Repeatability as a Limiting Parameter in Aircraft Development Force Measurements in Conventional and Cryogenic Wind Tunnels, AGARD FDP Symposium, Neapel, September 1987* (, 1987)

8.6 B.C. Carter: *Interference Effects of Model Support Systems, AGARD Rep. R 601* (AGARD,)

8.7 A. Pope, K.L. Goin: *High-Speed Wind Tunnel Testing* (Krieger, New York 1978)

8.8 G. Bridel: *Untersuchung der Kraftschwankungen bei einem querangeströmten Kreiszylinder, Dissertation, Nr. 6108* (ETH Zürich, Zürich 1978)

8.9 G. Schewe: A multicomponent balance consisting of piezoelectric force transducers for a high-pressure windtunnel, Techn. Messen **12**, (1982)

8.10 G. Schewe: On the force fluctuations acting on a circular cylinder in crossflow from subcritical to transcritical Reynolds numbers, J. Fluid. Mech. **133**, 265 (1983)

8.11 G. Schewe: *Force measurements in aerodynamics using piezo-electric multicomponent force transducers. Proc. 11th ICIASF '85 Record, Stanford Univ* (, 1985) p. 263

8.12 N.J. Cook: A sensitive 6-component high-frequency-range balance for building Aerodynamics, J. Phys. E. **16**, (1983)

8.13 H. Psolla-Bress, H. Haselmeyer, A. Hedergott, G. Höhler, H. Holst: *High roll experiments on a delta wing in transonic flow, Proc. 19th ICIASF 2001 Record, Cleveland, Ohio, Aug. 27-30 2001* (, 2001) p. 369

8.14 G. Schewe: Beispiele für Kraftmessungen im Windkanal mit piezoelektrischen Mehrkomponenten-meßelementen, Z. Flugwiss. Weltraumforsch. **14**, 32–37 (1990)

8.15 H. Triebstein, G. Schewe, H. Zingel, S. Vogel: Measurements of unsteady airloads on an oscillating engine and a wing/engine combination, J. Aircr. **31**(1), 97 (1994)

8.16 N. Schaake: *Querangeströmte und schiebende Zylinder bei hohen Reynoldszahlen, Dissertation* (Univ. Göttingen, Göttingen 1995)

8.17 G. Gautschi: *Piezoelectric Sensorics* (Springer, Berlin, Heidelberg 2002)

8.18 G. Schewe: Sensitivity of transition phenomena to small perturbations in flow round a circular cylinder, J. Fluid. Mech. **172**, 33 (1986)

8.19 G. Schewe: Reynolds-number effects in flow around more-or-less bluff bodies, J. Wind Eng. Ind. Aerodyn. **89**, 1267 (2001)

8.20 G. Schewe: *Reynolds-number-effects and their influence on flow induced vibrations, Proc. Structural Dynamics Eurodyn 2005* (Millpress, Paris 2005) p. 337

8.21 G. Schewe: Nonlinear flow-induced resonances of an H-shaped section, J. Fluid. Struct. **3**, 327–348 (1989)

8.22 D. Schimke, P. Jänker, V. Wendt, B. Junker: *Wind tunnel evaluation of a full scale piezoelectric flap control unit, Proc. 24th European Rotorcraft Forum, Marseille, 15-17. Sept. 1998* (, 1998)

8.23 G. Schewe, H. Mai, G. Dietz: Nonlinear effects in transonic flutter with emphasis on manifestations of limit cycle oscillations, J. Fluid. Struct. **18**, 3 (2003)

8.24 G. Dietz, G. Schewe, F. Kießling, M. Sinapius: *Limit-Cycle-Oscillation Experiments at a Transport Aircraft Wing Model, Proc. Int. Forum Aeroelasticity and Structural Dynamics 2003, Amsterdam* (, 2003)

8.25 G. Schewe, C. Steinhoff: Force measurements on a circular cylinder in a cryogenic-Ludwieg-tube using piezoelectric transducers, Experiments in Fluids , (2007)

8.26 H. Rosemann: The Cryogenic Ludwieg-Tube-Tunnel at Göttingen, AGARD Special Course. In: *Cryogenic wind tunnel technology*, ed. by (AGARD, 1997)

8.27 J. Tichy, G. Gautschi: *Piezoelektrische Meßtechnik* (Springer, Berlin, Heidelberg 1980)

8.28 F.G. Tatnall: *Tatnall on Testing* (American Society of Metals, Metals Park 1966)

8.29 K. Hoffmann: *An Introduction to Measurement using Strain Gages* (Hottinger Baldwin, Darmstadt 1989)

8.30 Measurement Group: *Strain Gage based Transducers* (Measurement Group, Raleigh 1988)

8.31 B. Ewald: Multi-component force balances for conventional and cryogenic wind tunnels, Meas. Sci. Technol. **11**, 81–94 (2000)

8.32 K. Hufnagel, B. Ewald: Force testing with internal strain gage balances, AGARD FDP Special Course, AGARD R-812. In: *Advances in Cryogenic Wind Tunnel Technology*, ed. by (AGARD,)

8.33 M. Dubois: *Feasability Study on Strain Gage Balances for Cryogenic Wind Tunnels at ONERA, Cryogenic Technology Review Meeting, NLR Amsterdam, September 1982* (,)

8.34 K. Hufnagel, : *A new Half-Model-Balance for the Cologne-Cryogenic-Wind-Tunnel (KKK), The Second International Symposium on Strain Gauge Balances, Mai 1999, Bedford* (TU Darmstadt, Darmstadt 1999)

8.35 G. Dietz, G. Schewe, H. Mai: Experiments on heave/pitch limit-cycle oscillations of a supercritical airfoil close to the transonic dip, J. Fluid. Struct. **19**(1), 1–16 (2004)

8.36 H. Hönlinger, J. Schweiger, G. Schewe: *The use of aeroelastic windtunnel models to prove structural design methods, Proc. No. 403 of the 63rd SMP Meeting of AGARD, Athens, Greece* (, 1986) pp. 9–1–9–15

8.37 G. Schewe: *Force measurements in aeroelasticity using piezoelectric multicomponent transducers, Intern. Forum Aeroelasticity and Structural Dynamics 1991 Aachen, DGLR-Bericht 91-06* (DGLR, Bonn 1991)

8.38 H. Zingel, : *Measurement of steady and unsteady airloads on a stiffness scaled model of a modern transport aircraft wing. Proc. Int. Forum on Aeroelasticity and Structural Dynamics, Aachen, DGLR-Bericht 91-06* (DLRG, Bonn 1991) p. 120

http://www.springer.com/978-3-540-25141-5

Springer Handbook of Experimental Fluid Mechanics
Tropea, C.; Yarin, A.; Foss, J.F. (Eds.)
2007, XXVIII, 1557 p. 1240 illus. in color. With DVD.,
Hardcover
ISBN: 978-3-540-25141-5